Microscopic visualisation of succinate producing biofilms of *Actinobacillus succinogenes.*

Sekgetho C Mokwatlo

July 12, 2017

Microscopic visualisation of succinate producing biofilms of *Actinobacillus succinogenes.*

by

Sekgetho Charles Mokwatlo

Dissertation presented in partial fulfilment of the requirements for the degree of

Master of Engineering in Chemical Engineering

at the University of Pretoria

Faculty of Engineering, Built Environment and Information Technology

Department of Chemical Engineering

University of Pretoria

Supervisor: Prof. W. Nicol

February 2017

Synopsis

Biofilms of *Actinobacillus succinogenes*, grown in a biofilm reactor system, were investigated for structure and cell viability, through microscopic visualisation with a confocal scanning laser microscope (CSLM) and a scanning electron microscope (SEM). Biofilms were sampled and visualised at steady state conditions with the broth containing succinic acid titres between 15 and 21 g/L. All sampled biofilm was 6 days old.

Six-day-old biofilms of *A. succinogenes* showed a heterogeneous biofilm architecture composed of cell micro-colony pillars which varied considerably in thickness, area and shape. Microcolony pillars consisted of a densely packed entanglement of sessile cells. Quantitative analysis revealed that the pillars were mostly large, with a mean pillar diameter of 170 μm and a mean thickness of 92 μm, although pillar diameter and thickness were variable as they ranged from 25 – 500 μm and 30 – 300 μm, respectively. In the regions close to the substratum surface, pillars were characterised by having defined borders with a network of channels ranging from 40 – 200 μm in width separating them. However, towards the middle of the biofilm depth some of the pillars coalesced. For this reason low cross sectional area coverage of biofilm consistently occurred at the bottom portion of the biofilm whilst the highest coverage was in the middle portion of the biofilm.

Regarding cell morphology, very large differences were observed. Planktonic cells were rod-shaped, whereas sessile cells expressed an elongated rod morphology and thus were much longer and thinner compared with planktonic cells. Planktonic

cells were 1 – 2 µm thick and 4 – 5 µm long, while sessile cells were 0.5 – 1 µm thick and 5 – 100 µm long. Long sessile cells resulted in extensive tangling in microcolony pillars, which may have contributed to the structural stability of the pillars. Fibre-like connections of constant diameter were observed between cells, and between the cells and surface. The diameter of these connections was approximately 20 – 30 nm.

Viability stains showed that in the bottom portion (from 0 - 20 µm above the substratum surface) of the biofilm, most of the cells were dead. However, the portion of covered area attributed to living cells increased past the middle of the biofilm towards the top part of the biofilm. A high percentage of living cells was thus found towards the top part of the biofilm. Overall, 65% (with 2% standard deviation) of the entire biofilm was composed of dead cells. In this way, the results show that operation at high acid conditions comes at a cost of low overall biomass productivity due to decreased active biomass.

Keywords: *Actinobacillus succinogenes*; biofilm structure; succinic acid; cell viability; cell morphology; confocal scanning laser microscopy; scanning electron microscopy.

Acknowledgements

Dedication

The following dissertation is dedicated to my late father, Ignatius Kgobokoane Mokwatlo, who passed away at the beginning of my Master's studies in the year 2016. I can never thank you enough for the support you have shown me throughout my entire education career. You gave me your best. To this day you continue to live in my heart.

Note on PDF navigation

All in-text references of figures, tables, sections and subsections in the PDF version of this dissertation are cross-referenced to their respective locations in the document by hyperlinks. The links are visible (in a red box).

Furthermore, when using Adobe Acrobat Reader, it is possible to return to the point from which the link was clicked by pressing the "Alt" and "Left arrow" keys together, or by following View → Page Navigation → Previous View in the menu bar.

Contents

List of Figures

ix

x

List of Tables

Nomenclature

1, 4-BDO	1,4 butanediol
bPCs	biobased platform chemicals
Cryo-SEM	cryogenic scanning electron microscopy
CSL	corn steep liquor
CSLM	confocal scanning laser microscopy
EM	electron microscopy
EPS	extracellular polymeric substances
ESEM	environmental scanning electron microscopy
GBL	γ-butyrolactone
HMDS	hexamethyldisilazane
HPLC	high-performance liquid chromatograph
MA	maleic anhydride
NADH	nicotinamide adenine dinucleotide
NADPH	nicotinamide adenine dinucleotide phosphate

OPPP	oxidative pentose phosphate pathway
PBT	polybutylene terephthalate
PEP	phosphoenolpyruvate
PTMEG	polytetramethylene ether glycol
PU	polyurethane
RI	refractive index
SA	succinic acid
SEM	scanning electron microscopy
TCA	tricarboxylic acid cycle
TEM	transmission electron microscopy
THF	tetrahydrofuran
YE	yeast extract

Chapter 1

Introduction

Most of fuels and platform chemicals today are derived from petroleum and natural gas. The strong dependence on fossil fuel reserves is dangerous as they are becoming depleted. Moreover, technologies used for their conversion contribute the most to global warming and present waste recycling issues. Therefore, in view of the ever-growing world population, and thus the increasing demand for energy and platform chemicals, a move is necessitated from society's dependence on these resources to renewable biomass-based resources. Such a transition is viewed by many as critical for the development of a sustainable industrial society, global warming management, and environmental management (Demirbas, 2009; Ghatak, 2011; Cherubini, 2010; Fitzpatrick *et al.*, 2010; Thomas 2009). Paramount to this move, however, is the development of the biorefinery concept.

Ideally, in biorefineries, different biomass feedstocks can be transformed through a range of white technologies and green chemistry to produce biofuels, bioenergy, biomaterials and biochemicals. This is analogous to refineries in the petrochemical industry where platform chemicals, fuels and energy are all products of crude oil resources. In biorefineries, however, waste generation will conceptually be avoided through integrated use of waste streams by other processes. Furthermore, due to the low thermal stabilities of biomass, white technologies will be used for conver-

sion, thus avoiding greenhouse gas emissions.

Of much concern, however, is the low energy content and seasonal availability of biomass resources, which may be limiting factors in the efficient supply of energy and fuels through biorefineries in the future. But this is not the case with the production of biobased platform chemicals (bPCs) as they require low volumes of biomass to meet demand (Fitzpratrick *et al.*, 2010). To illustrate this, in 2007, the market value of the chemicals industry in the US was comparable to that of the fuel industry (all derived from petroleum), although a lesser fraction of petroleum was used for the former (Fitzpratrick *et al.*, 2010). In this way, bPCs also provide an economic opportunity.

In a biorefinery context, bPCs can be produced by converting monosaccharides derived from treated lignocellulosic biomass material by either chemical synthesis or fermentation (Cherubini, 2010). Succinic acid (SA), listed as one of the top 12 most promising bPCs by the US Department of Energy in 2004, is currently commercially produced by various companies (e.g. Myriad, BioAmber, Reverdia & BASF-Purac) through fermentation. Most of the top 12 bPCs are main products in the metabolic pathways of many microorganisms, hence the popularity and the large body of research on fermentative production of bPCs with various microorganisms.

Economic production of these bPCs will be characterised by maximised productivities, titre, and yields of fermentation processes as well as by optimised feed compositions. In this view, high cell density fermentations are critical. This increases the concentration of cells, viewed as biocatalysts, in the fermenter, ultimately catapulting volumetric productivities. High cell densities in fermenters can be achieved by various cell-retainment strategies for suspended cell systems. However, these usually add to the capital and running costs of the process. On the other hand, some microorganisms can adhere naturally to available surfaces in the fermenter by forming a self-produced matrix called a *biofilm*. Biocatalyst concentrations in the biofilm far exceed those that can be attained with any form of cell-retainment strategy of suspended cells systems; this is evidenced by high volumetric productivities attainable with biofilm reactors in comparison with the

latter (Brink & Nicol, 2014; Cheng *et al.*, 2010; Qureshi *et al.*, 2005). Apart from the gain of high productivities, biofilms offer long-term operational stability and also improved tolerance to toxic substances (Gross *et al.*, 2007). Improved tolerance may indicate the possible direct use of low-cost, and often toxic, hydrolysate byproducts of lignocellulosic pre-treatment processes, without tampering much with the productivities of biofilms.

Of unique interest to this study, however, is the fermentative production of succinic acid by biofilms of the bovine rumen bacteria *Actinobacillus succinogenes*. This organism has been intensely studied by the Bioreaction Engineering Group at the University of Pretoria, which has been exploring steady-state metabolic flux distributions at various fermenter conditions (Bradfield & Nicol, 2014; Brink & Nicol, 2014; Herselman *et al.*, 2017), rate comparisons of biofilm and suspended modes (Brink & Nicol, 2014; Maharaj *et al.*, 2014) and fermentations of various sugar types, including hydrolysate streams (Bradfield & Nicol, 2016; Bradfield *et al.*, 2015). In summary, it is a high-productivity and high-yield process with industrial promise.

Although research efforts have advanced the understanding of this process to higher levels, the story of *A. succinogenes* yet remains incomplete. The productive aspect of these bacteria is just one side of the coin. It is becoming clear that the structure, physiology, and organisation of cell microcolonies within and throughout the biofilm matrix determine the productive behaviour of the biofilm. Regardless, to date, no studies on the biofilm morphology and cell viability states within *A. succinogenes* biofilms have been reported in the literature. The large body of research available on this biofilm process must be coupled with the study of the biofilm's morphology to present a complete and comprehensive picture.

Maintaining healthy biofilm is important for an industrial process of biobased SA production. Maharaj & Nicol (2014) observed that specific SA productivity (per biomass) decreased with increased concentrations of SA. This was attributed to possible changes in the composition of the biofilm (extracellualr polymeric substances vs cells) or in the fraction of the metabolically active cells within the biofilm. Therefore, it will be interesting to quantify the extent of cell death within

3

the biofilm matrix and, very importantly, the position of metabolically active cells across the depth of the biofilm. The activity of cells within these biofilms will determine the efficiency of the process as dead biomass will only serve to take up space in the fermenter.

Furthermore, Brink & Nicol (2014) confirmed variations in the content of extracellular polymeric substances (EPS) in the biofilm matrix of *A. succinogenes* at varying shear rate conditions. Variation in the EPS content signifies variation in the biofilm structure and thus in the emergent productive behaviour. Lastly, Bradfield & Nicol (2014) noted the distinct macroscopic appearance and form of *A. succinogenes* biofilms as functions of medium conditions, attached surface type, and fermentation history. As such, the influence of shear rates, acid concentrations and long term steady state operation on the physiological state of the *A. succinogenes* biofilms are all possible angles to explore which can assist in the understanding of this process.

The current research study is the first endeavour to investigate *A. succinogenes* biofilms through microscopic visualisation. For this purpose, shear rates, medium composition and steady state SA titre conditions in the fermenter, as well as fermenter operation period, were kept constant from run to run. This was done so that a baseline understanding of the biofilm structure and morphology could be established first, to precede future studies in which the role played by such factors can be explored.

Biofilms can be visualised using various microscopic techniques such as confocal scanning laser microscopy (CSLM), electron microscopy (scanning and transmission), light microscopy and atomic force microscopy to name a few. Among these techniques, it is CSLM that has advanced the current insight into biofilms the most (Costerton, 1999; Neu & Lawrence, 2015). CSLM permits non-invasive and in situ visualisation of hydrated biofilms, extracting optical sections of specimens without background halos and scatter information (Costerton, 1999). Coupled with image processing computer software, and environmentally and chemically sensitive fluorophores, distinctions between dead and live cells can be made, including 3D reconstructions of the biofilm. Significant progress has been made in under-

4

standing the structure of various biofilms and it has become clear that a generic description fails to encompass all the observations accordingly.

The objective of this study was to investigate, by means of microscopic visualisations, the biofilm structure formed by the bovine rumen bacteria *Actinobacillus succinogenes* 130Z, in a continuous biofilm reactor at steady state conditions. Six-day-old biofilms were sampled at steady state conditions, with the SA titre regulated between 15 and 21 g/L, without shear variation.

Biofilm was grown on both glass and plastic coverslips, in a novel biofilm chamber housing. Two separate external recycle lines were used; the first was used for agitation in the main fermenter, and the second for circulating the fermentation broth through the biofilm sample chamber. D-glucose was used as the organic carbon source at 40 g/L concentration, CO_2 as the inorganic carbon source, and yeast extract (YE) as well as corn steep liquor (CSL) as nitrogen sources. Biofilms were visualised using light microscopy, scanning electron microscopy, and CSLM. Live/Dead bacterial viability stains were used to distinguish between the active and inactive fractions of cells across the biofilm depth.

Chapter 2

Theory

2.1 Bio-based Succinic Acid

Succinic acid (SA) is a four-carbon dicarboxylic acid with the chemical formula $C_4H_6O_4$. It is predominantly produced from butane through the catalytic hydrogenation of maleic acid or maleic anhydride (Cok *et al.*, 2014). A ball and stick model of the SA molecule is shown in Figure 2.1.1.
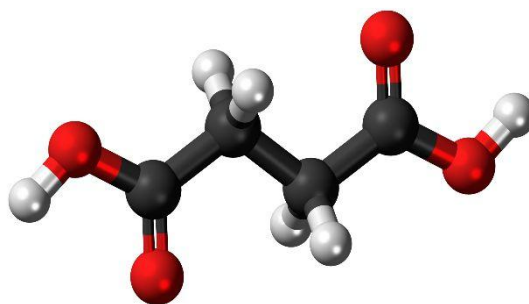
Figure 2.1.1: A 3D ball and stick diagram of the succinic acid molecule.

SA can serve as a building block for a plethora of chemicals, hence its inclusion in the list of the top 12 most important biobased platform chemicals by the US Department of Energy (2004). Because of the remarkable similarity of maleic

6

anhydride (MA) and SA chemicals, SA can serve as an attractive replacement for MA, which boosted a 1.85 million ton per year market in 2015 (Grand View Research, 2015). Alternatively, SA finds extensive application in the food, agricultural, chemical and pharmaceutical industries. Its most important application is possibly as an intermediate of 1,4-butanediol (1, 4-BDO). The market size of 1,4 BDO, which was estimated at USD 4.72 billion in 2013 (Grand View Research, 2015) is currently projected to reach USD 8.96 billion in 2020 (Markets and Markets, 2015) at a compound annual growth rate of 8.23%. The substrate 1,4-BDO is substantially used as an intermediate for tetrahydrofuran (THF),γ-butyrolactone (GBL), polytetramethylene ether glycol (PTMEG), polybutylene terephthalate (PBT), polyurethane (PU), and other solvents. These chemicals find widespread use in engineering plastics, fibres, medicines, artificial leather, cosmetics, pesticides, hardeners, plasticizers, solvents, and rust removers.

The prospect of producing biobased SA through fermentation has attracted overwhelming research interest. The intended result of such research interest is chiefly the replacement of petrochemical routes of producing succinic acid with improved and highly efficient biotechnological production routes. Rapidly diminishing petroleum resources, volatile oil prices and high carbon dioxide emissions are among the main incentives contributing towards the move from petrochemical routes. Furthermore, an increasingly growing market demand for biobased succinic acid makes such a quest desirable, seeing that the world is moving towards more energy efficient and greener technologies.

SA production in microorganisms occurs through the reductive branch of the tricarboxylic acid cycle (TCA). Identified biocatalysts for SA production are *Mannheimia succiniciproducens* (Lee *et al.*, 2002), *Anaerobiospirillum succiniciproducens* (Samuelov *et al.*, 1999), *Basfia succiniciproducens* (Scholten *et al.*, 2009), modified strains of *Escherichia coli* (Beauprez *et al.*, 2010) and *Actinobacillus succinogenes*. Among the wild type producers, *A. succinogenes* is considered the most promising, based on the extent of open literature publications. It is known for high acid titre tolerance, ability to utilise a wide range of carbon sources (Pateraki *et al.*, 2016) and ability to self-immobilise, thus forming biofilms, which assists in attaining high

7

cell densities without actively recycling cell mass. High cell densities have the advantage of significantly improving the productivities of bioreactors.

2.2 Metabolism of *Actinobacillus succinogenes* biofilms

Microorganism

A. succinogenes 130Z is a gram-negative, capnophilic, non-motile, non-spore forming pleomorphic coccobacillus isolated from the rumen of a cow at Michigan State University (Guettler *et al.*, 1999). It is a non-fastidious organism that grows well on blood-free media and it was also found to grow on chemo-organotrophic media. It is a facultative anaerobe, though its growth is enhanced at increased CO_2 concentrations as it is capnophilic (Guettler *et al.*, 1999) . It has been found to grow optimally within a temperature range of 37 °C to 39 °C and between pH 6.0 and pH 7.8. Its mixed acid fermentation results in considerable amounts of succinic acid, acetic acid and formic acid, and minor amounts of ethanol (McKinlay *et al.*, 2005).

Metabolic pathways considerations

An interesting characteristic of *A. succinogenes* is its ability to metabolise a wide variety of sugars, achieving relatively high SA titres, yields and productivity. This has also been demonstrated for unrefined sugar-rich streams from industry such as corn stover hydrolysates and cane molasses (Bradfield & Nicol, 2016; Liu *et al.*, 2007). The metabolisms of these sugars all link up to its central metabolism where succinic acid, acetic acid, formic acid, ethanol and/or pyruvic acid are excreted as metabolites.

Essentially, the pathways involved in the degradation of these sugars lead to the formation of phosphoenolpyruvate (PEP) via glycolysis. PEP is an intermediate in the central metabolism pathways of *A. succinogenes*, and serves as the node between the reductive branch of the TCA cycle (C4 pathway) and the oxidative

8

branch (C3 pathway) of the TCA cycle. The metabolic network of A succinogenes is given in Figure 2.2.1.

(1) phosphoglucose isomerase
(2) phosphoenolpyruvate carboxykinase (+ATP)
(3) pyruvate dehydrogenase
(4) pyruvate formate-lyase
(5) formate dehydrogenase
(6) pyruvate kinase (+ATP)
(7) phosphotransacetylase (+ATP)
(8) fumarate reductase (+2/3 ATP)

G6P Glucose -6-Phosphate
F6P Fructose-6-Phosphate
F1,6BP Fructose-1,6-Bisphosphate
DHAP Dihydroxyacetone Phosphate
G3P Glyceraldehyde-3-Phosphate
PEP Phosphoenolpyruvate
Ac-CoA Acetyl Coenzyme A
Ald Acetaldehyde
AcP Acetyl Phosphate

Figure 2.2.1: Central metabolic network of *Actinobacillus succinogenes.*

The C4 pathway is responsible for the production of succinate, whereas the C3 pathway results in the production of acetate and formate. In summary, the C4 pathway oxidises two nicotinamide adenine dinucleotide (NADH) molecules, and fixes one CO_2 molecule, for every succinate molecule formed. Therefore, channelling the flux towards the C4 pathway requires sufficient levels of CO_2 and reducing power (NADH). The organism manages to satisfy the redox balance by controlling the split of the carbon flux at the PEP node towards the C3 pathways and the C4 pathway as there is a net production of NADH in the C3 pathway. Equation 2.1 represents the overall pathway from glucose to succinic acid, which shows that there is a net consumption of CO_2 and NADH in the C4 pathway. Equation 2.2 to 2.4 represents the pathways to the metabolites formed in the C3 pathways where there is a net production of NADH.

9

$$\textbf{SA} : C_6H_{12}O_6(Glc) + 2NADH + 2CO_2 \rightarrow 2C_4H_6O_4(SA) + 2H_2O \tag{2.1}$$

$$\textbf{PDH} : C_6H_{12}O_6(Glc) + 2H_2O \rightarrow 2C_2H_4O_2(AA) + 2CO_2 + 4NADH \tag{2.2}$$

$$\textbf{PFL} : C_6H_{12}O_6(Glc) + 2H_2O \rightarrow 2C_2H_4O_2(AA) + 2CH_2O_2(FA) + 2CO_2 + 2NADH \tag{2.3}$$

$$\textbf{Pyruvate} : C_6H_{12}O_6(Glc) + 2H_2O \rightarrow 2C_3H_4O_3(PYR) + 2NADH \tag{2.4}$$
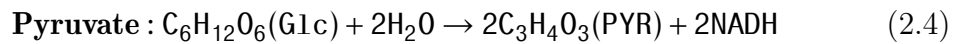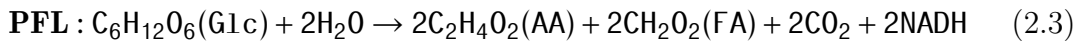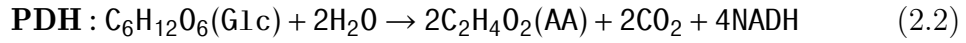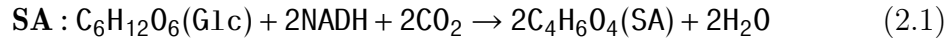
Theoretically, a maximum yield of succinic acid on glucose is 1.12 g/g. This yield is achievable in the case of a central metabolic network with a full TCA cycle and/or a glyoxylate shunt, with no biomass production. As can be seen from Figure 2.2.1 , *A. succinogenes* lacks a full TCA cycle and a glyoxylate shunt in its central metabolic network, and as such, redox constraints limit maximum succinic acid yield to either 0.66 g/g or 0.87 g/g for pyruvate conversion to acetyl-CoA by pyruvate formate-lyase or pyruvate dehydrogenase, respectively (Bradfield & Nicol, 2014). Formate can also be broken down by formate dehydrogenase, in which case the maximum yield is also 0.87 g/g.

Fermentation considerations

Rate and yield comparison for succinic acid production between suspended cells and biofilms was conducted in a continuous bioreactor (Brink & Nicol, 2014). Severe differences were observed as biofilms consistently achieved high productivity, yields and titre in comparison with suspended cells. This is attributable to order-of-magnitude-differences in the biomass concentrations of the biofilm and chemostat runs: in the biofilm runs where biofilm biomass concentrations ranged from 13 to 28 g/L, whereas the chemostat runs achieved a maximum biomass concen-

10

tration of 2.65 g/L. It was also shown that biomass growth is inhibited at and above SA titres of 10 g/L, where SA production is predominantly maintenance driven. In this region, biofilm growth does not halt completely but occurs at very low rates. Maintenance production of SA implies little loss of carbon to biomass, which means that SA yields are improved in this mode. Biofilm formation was shown to be rapid at high dilutions (>0.3 h^{-1}) where low acid conditions are prevalent (Brink & Nicol, 2014; Maharaj *et al.*, 2014).

Metabolic flux distribution of *A. succinogenes* has been studied in a continuous biofilm reactor at steady state operation (Bradfield & Nicol, 2014). It was found that a specific dilution rate did not relate to a specific glucose consumption rate, thus showing that the total and active biomass content in the bioreactor was dependent on the operational history of the bioreactor. Metabolic flux distribution was in fact related to glucose consumption rates as this was indicative of the total active biomass. The results signified that the selectivity of succinic acid was increasingly favoured by increasing glucose consumption, whereas formic acid production was decreased above a glucose consumption of 20 g/L, reaching zero at high glucose consumptions. The SA yield on glucose (0.90 g/g) exceeded the maximum yield obtainable in the ideal case that formate is not produced. Redox balances showed that the overproduction of SA was due not only to declines in formic acid production, but also to an additional source of NADH. The extra NADH was found to increase with increases in glucose consumption.

A similar study was also done by Bradfield & Nico (2016)l, this time with xylose as the carbon source. The same trend of increasing SA production with increased substrate consumption was observed, though lower yields, productivities, and titres were achieved. Extra production of NADH also increased with increased xylose consumption. Sufficient experimental evidence showed that the extra NADH was produced through the increased oxidative pentose phosphate pathway (OPPP) flux (relative to substrate uptake flux) (Bradfield & Nicol, 2016). The increased OPPP flux results in the increased production of nicotinamide adenine dinucleotide phosphate (NADPH), which can be converted to NADH by transhydrogenase in *A. succinogenes*, and thus finally used in the C4 pathway. Thus biofilms of *A.*

11

succinogenes are shown to be very favourable for high SA production.

The effect of CO_2 levels in the fermentation broth was investigated by Herselman *et al.* (2016) in a continuous biofilm reactor under steady state conditions. They identified three different steady state operating regimes depending on the amounts of dissolved CO_2 in the fermentation broth. SA productivities plateaued at and above 36.8% saturation level, and decreased (without flux shifting) below the same saturation level. Fluxes to the C4 were less favoured below CO_2 saturation levels of 17.1%. These findings highlighted that low saturation levels of 36.7% did not limit SA productivity, meaning that costs on effective CO_2 sparging can be saved.

2.3   Biofilm basics

Bacteria have mostly been studied as free-flowing cells in suspension (planktonic cells) yet they predominantly grow as sessile communities termed biofilms. More than 99% of microbes in nature are estimated to exist as biofilms (Donlan, 2009; Davey & O'Toole, 2000; Vu *et al.*, 2009).

Biofilms are 'structured communities of cells (mixed or pure species) embedded in a self-produced matrix of EPS adherent to inert or living surfaces' (Costerton, 1999). They may form as communities that are surface attached or as flocs, which are mobile biofilms that form in the absence of any substratum (Flemming *et al.*, 2016). Biofilm bacteria constitute a coordinated functional community more efficient than floating planktonic cells, made possible by the physiological cooperativity of bacterial cells in stable juxtaposition with cells of the same species (Fletcher, 1986).

Sessile bacteria have been shown to exhibit much dominant metabolic activity over planktonic bacteria. In addition, the cell densities of bacteria within biofilms (per volume of biofilm) have also been reported to be significantly higher than planktonic cell densities(per broth volume) (Costerton *et al.*, 1995). Characteristics of

biofilms include the ability to accumulate high cell densities by self-immobilisation, the physiological cooperativity, enhanced their metabolic activity, resistance to toxic reactants and long term stability (Gross *et al.*, 2007). These are properties which have made them either a nuisance or an advantage depending on the application.

Microorganisms which form biofilms have been the cause of persistent infections in plants, humans, and animals (Costerton *et al.*, 1987), as well as the cause of persistent contamination of medical devices and implants (Shirtliff & Leid, 2009). Moreover, biofilms are responsible for biofouling and contamination of process water equipment (Flemming & Wingender, 2010), and for microbially influenced corrosion (Little & Lee, 2014). In contrast, biofilms are exploited in industry as biocatalysts for the production of biofuels, bulk and fine chemicals, filtration of drinking water, and degradation of wastewater and solid waste (Flemming *et al.*, 2016).

In most biofilms, EPS are reported to constitute approximately 90% of the dry biomass of biofilms (Flemming *et al.*, 2016). Moreover, EPS are highly hydrated, consisting of approximately 95% of bound and unbound water (Dohnalkova *et al.*, 2010), and are made of mostly exopolysaccharides, fimbriae, pili, external DNA, lysed cells, proteins and nucleic acids. However, the components of the EPS can vary greatly between biofilms of different microorganisms. This variation also exists in pure species biofilms grown at different conditions. Nonetheless, it widely agreed that the gel-like EPS enable the biofilm mode of bacterial life; EPS are reported to provide the mechanical stability of biofilms, to mediate the adhesion of cells to surfaces, to immobilise biofilm cells and keep them in close proximity by forming a cohesive three-dimensional polymer network (Flemming *et al.*, 2016), and to protect sessile cells from desiccation by acting as a sorption matrix. The functions of EPS in biofilms are extensive and have been critically reviewed by Flemming *et al.* (2016).

Advancement in analytical imaging tools has enabled the revision of an early rendering on biofilms as "consisting of a homogenous distribution of cells in a uniform exopolysaccharide matrix" to that of significant variability and heterogeneity

13

(Yang *et al.*, 2000; Stewart *et al.*, 1993). Studies on living biofilms have shown variability in the distribution of cells and cell aggregates, their EPS matrix, and void spaces or water channels within biofilms (James *et al.*, 1993; Stewart *et al.*, 1993; Wolfaardt *et al.*, 1994). Moreover, it is important to highlight that biofilm heterogeneity and variability appears not to be the sole result of mixed cultures as pure cultures also possess many of the heterogeneity characteristics of mixed culture biofilms (Costerton *et al.*, 1995). The spatial arrangement patterns of these elements, often specific to each species, has been termed "biofilm architecture". The structure is dynamic and is mostly influenced by extrinsic factors such as shear stress, substrate availability, and diffusional limitations, and by intrinsic factors such as the composition of the EPS (which influences the cohesive strength of the biofilm matrix) and the growth rate of the biofilm cells

Thus far, three models of the biofilm structure have been proposed and a biofilm structure may reflect any of these models or any combination thereof

1. *Heterogeneous mushroom model*: in this biofilm structure a large microcolony of cells, elevated to the bulk fluid, is firmly attached to the substratum by a narrow stalk of biomass, thus the mushroom-like structure. Some of these mushrooms like structures coalesce, leaving water channels at the base of the biofilm (Costerton *et al.*, 1995). Moreover, smaller branching channels within microcolonies have also been observed, which has led to these channels being compared to a primitive circulatory system, providing an effective means of exchanging nutrients and metabolites with the bulk fluid phase and a means of achieving a degree of homoeostasis within microcolonies (Wimpenny & Colasanti, 2006).

2. *Heterogeneous mosaic model*: this is a patchy biofilm structure where the mushroom-like microcolonies are unconnected and well separated from their neighbours (Walker *et al.,* 1995). A background film of cells, less thick than microcolonies, covers the space in between the microcolonies. Because of the large spaces that exist between microcolonies, no water channels result in this structure.

14

3. *Homogeneous model:* This model describes flat and dense biofilm structures such as those encountered in dental plaques (Wimpenny & Colasanti, 1997). No water channels and significant protrusions from the surface are observed in this structure.

2.4 Microscopic visualisation techniques

The use of microscope tools to both visualise and analyse biofilms has significantly advanced the understanding of biofilms. Electron microscopy (EM), confocal scanning laser microscopy (CSLM), atomic force microscopy, and light microscopy are examples of microscopic techniques used by most researchers for studying biofilms. However, no single technique can give a complete picture of the biofilm, and the choice of type of techniques used mostly depends on the availability of the tools, and the type of study conducted. The techniques used in this study are discussed in this section.

2.4.1 Confocal Scanning Laser Microscopy

Confocal scanning laser microscopy (CSLM) is perhaps the most widely used technique in the study of biofilms (Neu & Lawrence, 2015). The technique was developed to overcome the challenges of out-of-focus blur encountered in conventional light and fluorescence microscopy. As an example, in fluorescence microscopy, 2D images may contain as much as 90% of fluorescence from out-of-focus planes which obscure fluorescence from the focused planes (Conchello & Lichtman, 2005). This out-of-focus blur seriously degrades the image by reducing its sharpness and contrast. Confocal microscopy eliminates background information through the use of point illumination and the placing of a detector pinhole in an optically conjugate plane. In this way, light emanating from out-of-focus planes is rejected by the detector pinhole, which only allows light very close to the point source.

CSLM is thus capable of extracting optical sections of specimens without back-

15

ground halos and scatter information, offering improved resolution in the axial and lateral directions as compared to conventional light and fluorescence microscopy (Shotton, 1989; Cerca *et al.*, 2012). In this way it allows a non-destructive, in situ and accurate examination of the internal detail of fully hydrated biofilms, without the use of harsh chemical fixations and embedding techniques. Coupled with computerised control of the microscope stage in the Z direction, a series of digital XY optical sections (a stack) can be automatically collected and processed to build a 3D reconstruction of the biofilm. Thus CSLM allows a four-dimensional (4D) analysis of biofilms (X, Y, Z, t). Moreover, its episcopic nature allows examination of biofilms cultivated on various non-transparent substrates, thereby broadening the types of analyses that can be performed (Costerton, 1985).

There have been many achievements in the research of biofilms with CSLM (Neu & Lawrence, 2015). CSLM allows the visualisation of the general biofilm structure (architecture) with voids and 3D surface topographies showing different morphological structures. The distribution of the EPS matrix within biofilms, as well as the identity of the matrix constituents, have been studied with CSLM (Neu & Lawrence, 2015). The biofilm development process has been studied by semi-continuously imaging temporal changes, from inoculation to maturation, of the biofilm grown in flow cell reactors. Moreover, cell activity and overall biofilm activity can also be studied using various Live/Dead bacterial viability staining kits. Environments that exist in the biofilm have been visualised with CSLM using environmentally and chemically sensitive fluorophores[1], revealing pH gradients, nutrient gradients, and metabolite gradients within the biofilm (Neu & Lawrence, 2015). These achievements have been brought about using CSLM along with sensors which can extract structural aspects, chemical cues and diffusivity. In this study biofilm structural aspects were investigated by using DNA staining fluorophores, SYTO9 and Propidium Iodide. These stains are also used to reveal cell activity within the biofilm.

---

[1]A fluorophore is a fluorescent chemical compound that can re-emit light upon light excitation. It can be used as a tracer in fluids, as a probe (when its fluorescence is sensitive to the environmental conditions), or as a dye for staining certain structures (nucleic acids, antibodies, peptides). They are notably used for staining cells in fluorescent imaging.

Because CLSM produces accurate images, by exclusion of out-focus blur, the digital images it produces are often used in quantitative analysis of biofilms through image processing software, enabling the computing of biofilm descriptive parameters such as maximum thickness, thickness distribution, and area coverage. Quantification of biofilm descriptive parameters removes subjective analysis of images based on visual inspection, and allows for comparison of research findings by other researchers. In this respect, Kober *et al.* (1993) described a method that determines the minimum sampled biofilm area that would be representative of the biofilm when doing quantitative analysis. Determination of this area ensures that conclusions arrived were based on the analysis of sufficient area that is representative of the biofilm investigated.

2.4.2 Electron Microscopy

Electron microscopy (EM) is an imaging technique which offers high resolution and hence higher magnification. Thus EM is an effective tool used for gathering detailed insight into features of the immediate surroundings of microorganisms and their ultrastructural nature (Dohnalkova *et al.*, 2011; Alhede *et al.*, 2012). Several EM techniques exist, which include scanning (SEM), transmission (TEM), and environmental scanning electron microscopy (ESEM).

With SEM, a finely focused electron beam scans the surface of a specimen to produce an image, and because of its high depth of field, the resulting image is three dimensional. Because of its ability to clearly visualise spatial relationship of sessile cells, SEM is a predominant electron microscopy technique used for biofilm investigation. With TEM, the internal cross-sectional detail of the individual sessile cells and their relationship to each other, as well as the overall biofilm, can be visualised. ESEM is a modified version of SEM which allows examination of fully hydrated biofilms or biological specimens.

Traditionally, biological sample preparation techniques for electron microscopy are harsh and introduce artefacts which can often be misinterpreted, resulting in

17

wrong conclusions being drawn (Wu *et al.*, 2014). Conventional biological sample preparation for SEM and TEM include fixation, dehydration, and drying. The role of chemical fixation is to halt cellular activity while preserving the internal 3D organisation, shape and size of the sample. Nonetheless, chemical fixation is known to result in considerable biofilm shrinkage, while dehydration with organic solvents is reported to remove certain components of the EPS and induce distortion of delicate structures such as membrane-associated vesicles (Dohnalkova *et al.*, 2011; Alhede *et al.*, 2012; Hunter & Beveridge, 2005; Little *et al.* 1991). with regard to biofilm investigations, conventional SEM preparation methods have been shown to expose the surfaces of sessile cells within biofilms as the hydrated EPS matrix collapses (Dohnalkova *et al.*, 2011; Alhede *et al.*, 2012; Little *et al.*, 1991; Hunter & Beveridge, 2005). Many researchers have reported the presence of thin fibre-like material connections between cells (Little *et al.*, 1991; Wu *et al.*, 2014; Alhede *et al.*, 2012). However, whether this is collapsed EPS matrix is still not certain (Alhede *et al.*, 2012).

The introduction of cryo-SEM has enabled the imaging of biofilms in the nearly fully hydrated state and closest to the natural state, without the effects of harsh chemical fixatives, dehydration and drying (Dohnalkova *et al.*, 2011). With cryo-SEM, samples are rapidly vitrified at high pressure to prevent ice crystal growth and are imaged at sub-zero temperatures. This method allows visualisation of the hydrated EPS matrix, though the internal components of the EPS matrix cannot be visualised. Also, with cryo-SEM, frozen samples melt and crack at high magnification due to the heat generated by the electron beam, overall this results in poor resolution (Alhede *et al.*, 2012).

Environmental SEM, however, requires no sample preparation. Wet biofilm samples can be directly visualised soon after they have been sampled. Thus, ESEM and cryo-SEM together allow the visualisation of the biofilm matrix closest to the "in situ" state, where sessile cells are unexposed but covered with the hydrated EPS matrix.

18

Chapter 3

Experimental

3.1 Bacteria and growth conditions

The microorganism used in this study is *Actinobacillus succinogenes* 130Z (DSM No. 22257; ATCC No. 55618), from the German Collections of Microorganisms and Cell Cultures (Braunschweig, Germany). Pure stock cultures were frozen at -40 °C in a 66% (vol) glycerol solution for long life storage in a freezer, this was after the viability and purity of the culture had been confirmed.

Inoculum was prepared from the frozen stock cultures by inoculating the culture in 15 mL of tryptone soy broth, stored in 25 mL screw-cap vials, and incubated at a rotation speed of 150 rpm and a temperature 37 °C for 16-20 hours. After this period, the broth was sampled and run through a high performance liquid chromatograph (HPLC) (Agilent Technologies, USA) for analysis. The presence of lactic acid and/or ethanol was indicative of an infection and the absence of succinic acid signified that the culture was non-viable. Viable culture broth's were stored at 7 °C and used within a week.

3.2 Biofilm growth media

The composition of the fermentation medium used for *A. succinogenes* was based on that of Urbance et al. (2003). All chemicals were obtained from Merck KGaA (Darmstadt, Germany) unless otherwise stated. The medium was made up of three parts: the nutrients solution, a phosphate buffer and the glucose solution. The nutrients solution was composed of 10 g/L of clarified corn steep liquor (CSL, Sigma Aldrich, St. Louis, USA), 6 g/L of yeast extract (YE), 1 g/L of NaCl, 0.2 g/L of MgCl•6H_2O, 0.2 g/L of CaCl$_2$•2H_2O, and 10 mL/L of Antifoam SE-15 (Sigma Aldrich, St. Louis, USA). The phosphate buffer consisted of 3.2 g/L KH$_2$PO$_4$ and 1.6 g/L K$_2$HPO$_4$. The glucose concentration was kept at 40 g/L. CO_2 was bubbled into the bioreactor at 10 vvm.

The CSL was clarified by autoclaving a 200 g/L solution of CSL and distilled water for 21 minutes at a temperature of 121 °C. The solids in the boiling solution of CSL were allowed to precipitate as the solution was cooled. The supernatant was used for the growth medium once it had cooled down, and the remaining supernatant was stored at 7 °C.

During the preparation of the fermentation medium, three separate solutions were prepared and were only mixed after autoclaving at 121 °C for 60 minutes. Combining the solution before autoclaving results in unwanted reactions occurring during autoclaving. Solutions were mixed aseptically once they had cooled down. This was done through the silicon tubing that connected the bottles, although these were clamped shut during autoclaving to prevent mixing.

3.3 Fermentation setup

The aim of this study was to investigate the biofilms formed by *A. succinogenes* when grown in a fermenter for the production of succinic acid. In this respect, it was necessary for the analysed biofilm to be developed in the conditions of a

fermenter, and to be sampled without contaminating the fermenter. This therefore required the use of bioreactors able to incorporate a biofilm growth surface that will be easy to use for microscopic preparations and subsequent visualisation, and that could be sampled aseptically.

For this reason the fermentation setup was constructed based on the design developed by Bradfield and Nicol (2014), which had been used for a succinic acid production study with biofilms of *A. succinogenes*. However, additions were made to the design to make it suitable for this study as discussed below.

Bioreactor system

The setup consisted mainly of the bioreactor body, media storage, tubing, and electrical components for automation and the online monitoring system (see Figure 3.3.1). The bioreactor body is composed of a glass cylindrical body (170 mm long, and 56.6 mm ID) fitted between an aluminium base and head, connected by an external recycle line for agitation. The external recycle line was kept as short as possible so that the broth conditions in the recycle line would be the same as those in the main fermenter. Four wooden sticks covered with terry cloths were used for biofilm attachment in the bioreactor.

The inside of the aluminium base was fitted with a circular gas distributor, which helps to break CO_2 bubbles and thus improve mass transfer of CO_2 into the liquid phase. CO_2 is required as it is fixed by *A. succinogenes* to make succinic acid.

A Tophit CPS417D glass probe (Endress+Hauser, Gerlingen, Germany), housed within an aluminium probe holder and connected in-line with the recycle stream, measured both temperature and pH. Temperature was controlled at 37 °C using measurements from the glass probe and the hot plate. The pH was controlled at 6.8 by dosing with a 10M NaOH solution in an On-Off fashion. Both the temperature and pH control process were automated via a custom-developed Labview program (National Instruments).

There are four main reservoirs connected to the reactor, namely;(1) the feed medium reservoir; (2) the NaOH reservoirfor pH control; (3) the antifoam reservoir

21

to help minimise foaming; and (4) the product collection reservoir. A foam trap bottle is also connected to the head of the bioreactor, which provides a vent for the supplied CO_2 and aids in foaming control. All the reservoir vents, including that for the foam trap and the CO_2 gas inlet line, were fitted with 0.2 μm PTFE membrane filters (Midisart 2000, Sartorius, Göttingen, Germany). Silicone tubing connected the reactor to components of the fermentation setup and marprene tubing was used for the peristaltic pump sections.

The line from the medium reservoir to the reactor included a sterile couple. One-half of this couple connection was fixed to the medium reservoir,and the other half was connected to the main reactor. The sterile couple made it possible to autoclave the reactor and medium reservoir separately, and to replenish aseptically the fermentation medium. Other components of the fermentation setup included the heating plate, a gas flow controller, and instrumentation devices used for the automation of pH and temperature control.

Addition: Biofilm sample chamber

Three biofilm chamber designs were implemented, but only one proved successful. In this section the design that was finally used for studying the biofilm is discussed.

Biofilm was grown in a biofilm sample chamber connected to the main bioreactor body by an additional external recycle stream (see Figure 3.3.2). The external recycle stream ensured that the fermentation broth in the main bioreactor was continuously circulated through the biofilm sample chamber. Pump speeds on both external recycle lines were such that the average linear velocity in the bioreactor and the biofilm sample chamber were the same. The total volume of the bioreactor and sample chamber (including tubing) was 390 mL with the sample chamber occupying only 13% of the total volume. All this ensured that conditions in the sample chamber closely mimicked those in the bioreactor. Temperature was also controlled at 37 °C in the sample chamber.

The sample chamber is similar in design to the bioreactor body but smaller (see Figure 3.3.3). The cylindrical glass fitted between an aluminium base and head is

22

115 mm long with an inside diameter of 37.5 mm. Two half-rod moulds were made to introduce dead volume within the cylindrical glass, leaving a 5 mm x 37 mm rectangular cross-sectional hollow in the centre for fluid flow. This considerably reduced the active volume of the sample chamber.

Biofilm was grown on both glass (Sigma Aldrich) and plastic (Thermanox) coverslips. The plastic cover slips were circular with a diameter of 13 mm, and the glass coverslips were square and rectangular at 24 mm x 24 mm and 50 mm x 24 mm respectively. On one flat side of the half-rod mould, one rectangular glass coverslip and four circular plastic coverslips were attached, and on the other flat surface two square glass coverslips and four circular plastic coverslips were attached. Glass coverslips were used for CSLM visualisation, while plastic coverslips were used for both SEM and CSLM (see Figure 3.3.4).

Figure 3.3.1: A simplified schematic of the fermentation setup.
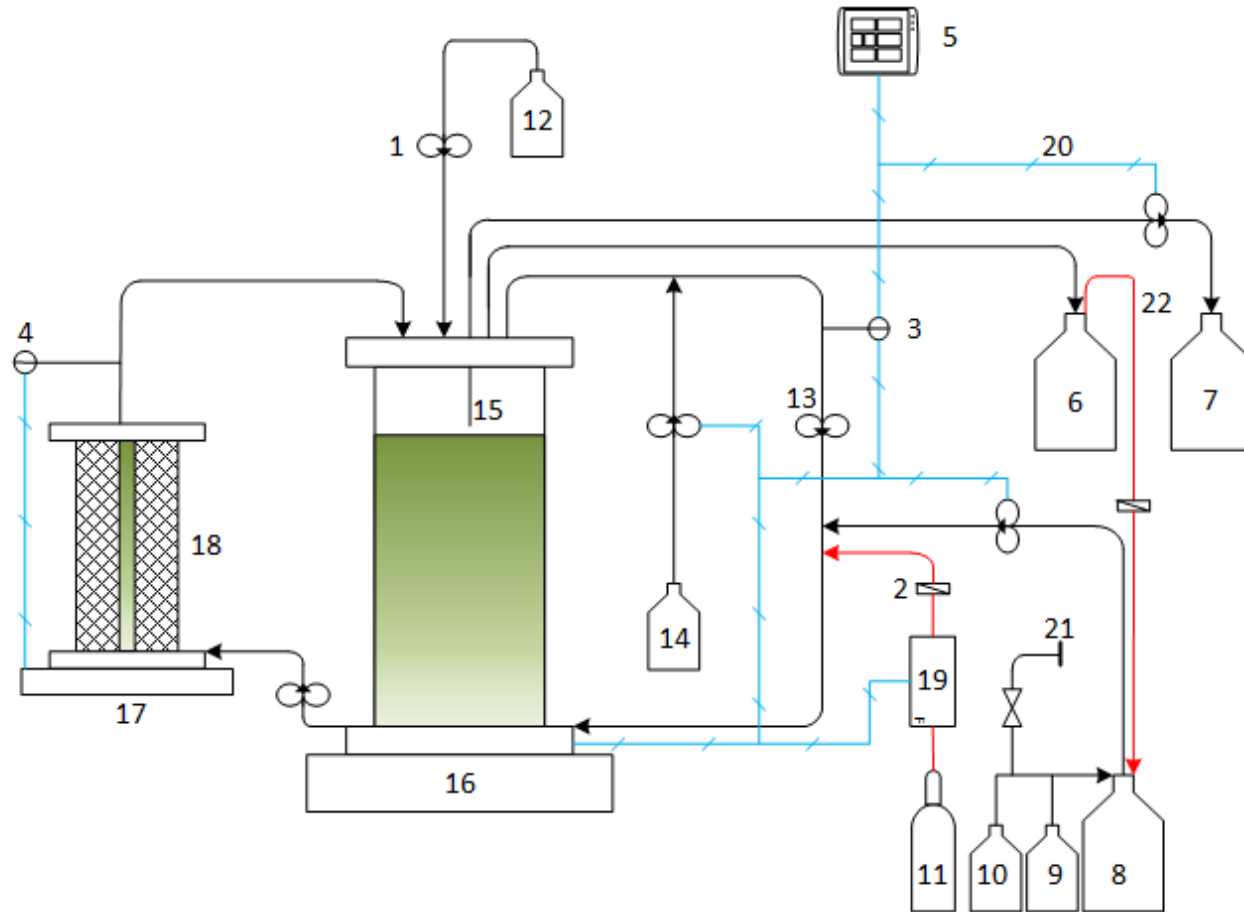
1. Peristaltic pump
2. Gas filter
3. pH and Temperature probe
4. Thermocouple
5. DAQ/PC control unit
6. Foam trap
7. Product reservoir
8. Medium reservoir
9. Glucose bottle
10. Phosphate bottle
11. CO2 cylinder
12. Antifoam reservoir
13. Recycle pump
14. NaOH reservoir
15. Bioreactor body
16. Hot plate
17. Hot plate
18. Biofilm sample compartment
19. Mass flow controller
20. Signal line
21. Feed transfer coupling
22. CO2 recycle line

Figure 3.3.2: The main bioreactor body and the biofilm sample chamber.
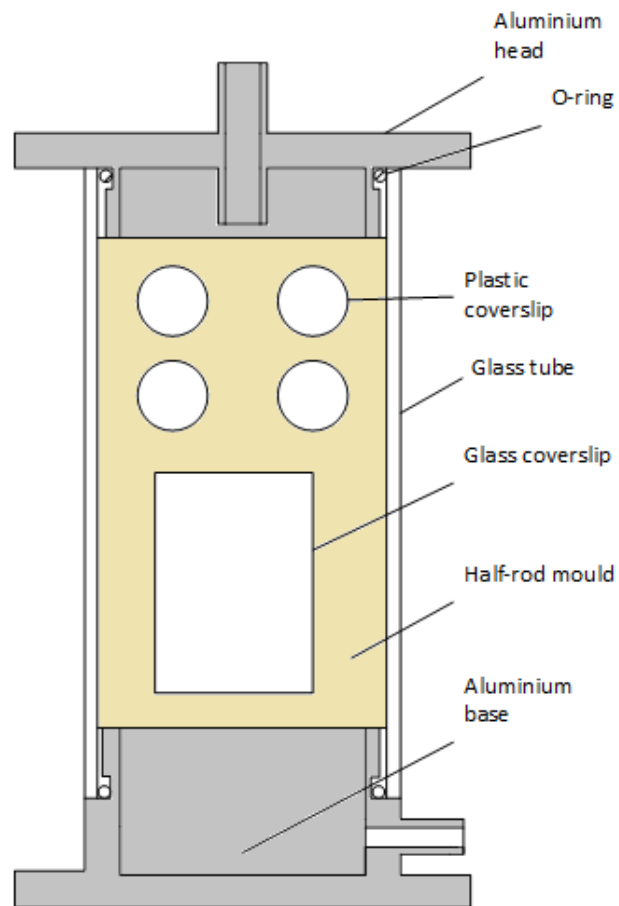
Figure 3.3.3: Schematic diagram of the cross- sectional view of the biofilm sample chamber.
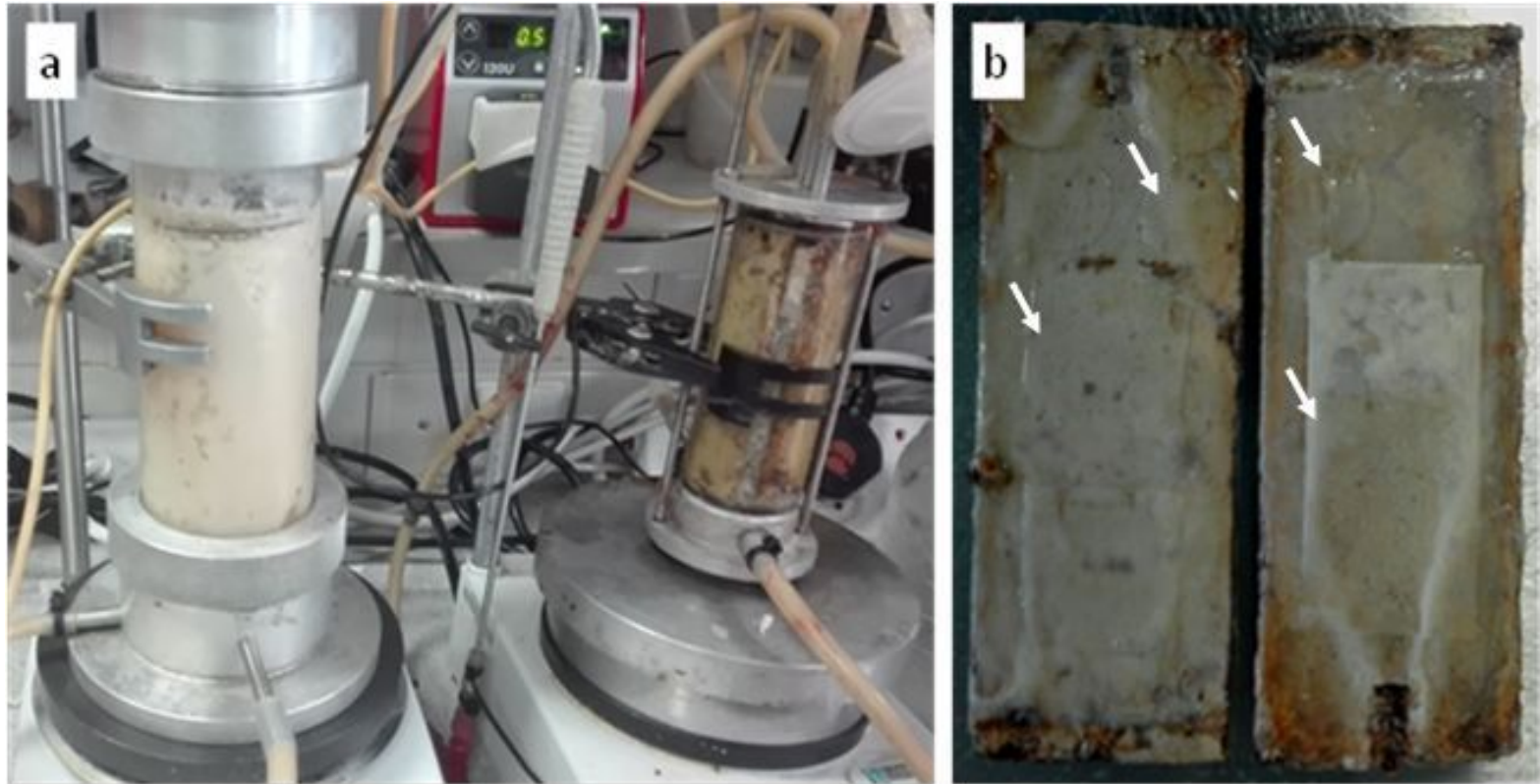
Figure 3.3.4: Biofilm accumulation on the glass surface of the bioreactor and sample chamber (a), and internals of the sample chamber after sampling, showing biofilm grown on rectangular glass coverslips and circular plastic coverslips (b).

Figure 3.3.5: Biofilm accumulation on the wooden sticks at the termination of the fermentation run.

3.4 Summary of biofilm development

In all, there were six biofilm sampling opportunities. The first three were done with the initially implemented biofilm chamber design, where biofilm was grown inside silicon tubes. In this case, the curvature of the silicon tubes did not permit proper mounting of the sample for microscopic examination. For this reason the design was discontinued. However, it was during this attempt that the correct stain concentrations were determined by using biofilm found on the inside of the silicon tube walls and smearing it onto microscope slides. Images acquired in those first three runs are not discussed in this study. The last three biofilm samples were obtained with the final design that was implemented, which is described in Section 3.3. These final three runs are henceforth referred to as runs 1–3.

CSLM data were obtained in runs 1, 2 and 3. All three runs had similar broth conditions (see Table 3.1) and start-up histories. The total acquisition area of sample 3 greatly exceeded the acquisition areas of samples 1 and 2 since these were part of the method development phase. Accordingly, only sample 3 data were used for quantitative analysis. However, some of the images generated from samples 2 and 3 were used in the qualitative (visual) analysis of the biofilm. The underlying assumption was made that samples 1, 2 and 3 shared the same basic morphology given the almost identical preparation procedure.

Table 3.1: Steady state acid titres prior to biofilm sampling

Sample no.	Succinic acid (g/l)	Acetic Acid (g/L)	Formic Acid (g/L)
Sample 1	18.1±0.6[1]	6.2±0.2	2.9±0.2
Sample 2	15.4±0.2	6.3±0.1	3.1±0.2
Sample 3	21.5±0.3	6.9±0.3	3.4±0.2

[1] Standard deviation of three samples over a period of 24 h, with a minimum of 6 h in between. Starting glucose concentration of 40 g/L.

29

Procedure

At the start of fermentations, feed was first prepared as discussed in Section 3.2. The non-electrical part of the fermentation setup, excluding the sodium hydroxide reservoir, was autoclaved at 121 °C for 60 minutes. Although it was possible to autoclave the entire setup at once, feed was autoclaved first and separately from the reactor body as it took a long time to cool down. This ensured that the pH probe in the aluminium holder did not stay dry for extended periods as this could damage it. After the couple connection between the feed medium and the bioreactor had been sterilised for 20 min in hot oil at 140 °C, the bioreactor was filled with medium together with the biofilm sample chamber.

The reactor was first run in batch mode for a day without inoculating. During this period it was determined whether the fermentation start-up process had been successful without an infection or contamination of the system. Once sterility of the system had been confirmed, a 10 mL inoculum was injected aseptically into the bioreactor. After inoculation, the batch mode operation was resumed for 24 h to build up cell mass. Fermenter mode was then switched to continuous at 0.1 h^{-1} dilution rate to build up biofilm without removing too many cells. The dilution rate of 0.1 h^{-1} was maintained for 24 h and was subsequently increased to 0.3 h^{-1} for a period of 48 h to further encourage biofilm formation. At this point, considerable biofilm formation was observed on the glass surface of the bioreactor, and on the surface attachment internals in the bioreactor. Thereafter, the dilution rate was dropped to 0.1 h^{-1} with the aim of attaining steady state at 15–21 g/L succinic acid. On average, it took 24 h of operation at 0.1 h^{-1} to reach steady state, and this was further maintained for a day before the biofilm was sampled. The same bioreactor operation procedure was followed for every run to ensure that all sampled biofilms were grown at similar conditions.

The flow from the bioreactor to the sample chamber, and from the sample chamber to the bioreactor was shut off by closing valves on the connection couples. This allowed aseptic removal of the biofilm sample chamber. Biofilm sample coupons were then carefully removed from the biofilm sample chamber and immediately immersed in a phosphate buffer solution at 37 °C to avoid desiccation. The samples

were then prepared for microscopic examination.

3.5 Microscopic techniques

CSLM

Sample coupons were removed from the biofilm sample chamber and immersed in a phosphate buffered saline (PBS) solution (at 37 °C) inside the wells of a six-well plate for 5 min. The PBS solution was replaced twice from the well. This was done carefully to avoid eroding biofilm from the coverslip surface. Samples were then stained for 30 min using Baclight LIVE/DEAD bacterial viability (Thermofisher Scientific, USA) stains at the recommended staining concentrations and a temperature of 37 °C. This stain consists of SYTO 9 and propidium Iodide to differentiate between vital and dead cells. It should be noted that in this document, when the term "dead" is used with regard to cells, this will be referring to cells with compromised membranes as the term dead is difficult to prove with cells.

Samples were examined on an LSM 510 Meta laser scanning confocal microscope (Zeiss, Germany). Images were acquired with LSM Image Examiner software and were further processed with a ZEN 2.3 lite image processor and ImageJ. The main objectives used were the Plan-Neofluar 10x/0.3, the Plan-Neofluar 40x/1.3 Oil DIC, and the Plan-Apochromat 63x/1.4 Oil DIC. A 488 nm excitation wavelength was used and emission fluorescence was collected at 635 nm (red) and 500 nm (green).

Scanning Electron Microscopy

Once the biofilm sample coupons had been removed from the sample compartment, they were washed with 0.075M sodium phosphate buffer. The samples were fixed with a 2.5% glutaraldehyde/formaldehyde mixture for 1 h.

After fixing, the samples were then washed again with a buffer solution and post-fixed with a 1% osmium tetroxide solution for 1 h. They were then dehydrated

through a series of graded alcohol solutions (30%, 50%, 70%, 90%, and 100%). The samples were then washed with a 50% (vol) ethanol and hexamethyldisilazane (HMDS) mixture, and finally dried in the HMDS solution. This type of drying is a chemical alternative to critical point drying, as it avoids the development of high tensions and consequent cracking in the drying biofilm. Subsequent to drying, the biofilm was coated with carbon in a Carbon Coater (Emitech K950X, England, Ashford). The coated samples were then visualised with a Zeiss Crossbeam 540 SEM (Zeiss, Germany, Oberkochen).

3.6   Analytical Methods

Metabolite analysis

Concentrations of glucose, ethanol and organic acids were analysed for with the HPLC. An Agilent 1260 Infinity HPLC (Agilent Technologies, USA) equipped with a refractive index (RI) detector and a 300 mm × 7.8 mm Aminex HPX-87H ion exchange column (Bio-Rad Laboratories, USA) was used. Two mobile phases were used for two methods of analysis. The first method consisted of a 0.02 M H_2SO_4 mobile phase solution fed at a flowrate of 0.6 mL/min and the second method used a 0.005 M H_2SO_4 mobile phase solution at the same flowrate. The second method was used to separate the phosphates from the glucose peak, as these were combined in the first method.

Quantitative image analysis

All the acquired image stacks for sample 3 were processed with the COMSTAT program (MATLAB ©) to give a quantitative analysis of the biofilm. The quantitative parameters analysed for are maximum thickness, average thickness, biomass cross-sectional area as function of depth, biofilm surface to volume ratio, and the roughness coefficient of the biofilm.

Prior to the performance of a quantitative analysis of the biofilm structure, it was

necessary to determine a minimum biofilm sampling area that is representative of the biofilm. Korber *et al* (1993) conducted an experiment in which they plotted a variation of a suitable biofilm parameter, which represented the heterogeneity of the biofilm, against increasing biofilm sampling area. In this way, a biofilm sampling area region where the variation in that parameter was relatively negligible was determined, which meant that the parameter became independent of the sampling area beyond the said region. In this way the minimum sampling area that is representative of the biofilm was determined. Korber *et al* (1993) found that for *Pseudomonas fluorescens*, and when using cell coverage as a determinative parameter, an area of 1×10^6 μm^2 was representative. Venugopalan *et al* (2005) determined that a minimum area of 2×10^5 μm^2 was representative for biofilms of *Sphingomonas* sp. strain L138, when using area coverage as a determinative parameter.

The representative biofilm sampling area for *A. succinogenes* was determined using the method described by Venugopalan *et al* (2005). This was done by computing substratum area coverage over a total area of 4.24×10^6 μm^2 in sample 3. Five substratum optical section images from five image stacks, acquired with a Plan-Neofluar 10x/0.3 objective lens, were used. Each digital image was divided into 8 octants, and each area of an octant was analysed as if it were a separate image. Using a self-written MATLAB program, 2,3,4,5...40 octants were randomly selected (depending on the sampling area) and the average substratum coverage values were computed. For each area eight measurements of the average substratum coverage were made. The result indicated that a representative biofilm sampling area for *A. succinogenes* is 2×10^6 μm^2 as can be seen in Figure 3.6.1.
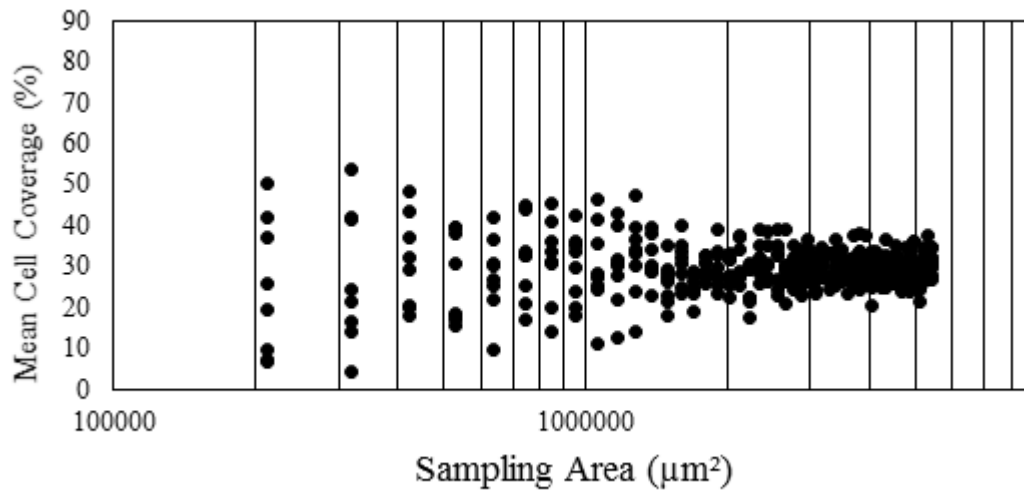
Figure 3.6.1: Determination of the biofilm sampling representative area for *A. succinogenes*. After an area of *2x10^6* μm^2 the band for mean cell coverage becomes constant.

Thus, the acquired area of 4.24x10^6 μm^2 for five image stacks was more than enough to do quantitative analysis of where the area of analysis would be representative of the biofilm. The parameters which were computed with COMSTAT are defined below with a brief explanation of the calculation method.

1. **Maximum thickness**: this is the thickest piece of the biofilm considering holes and cavities in the structure, this is, therefore, the highest point of the biofilm in relation to the substratum surface less the empty space (Heydorn *et al.*, 2016). This is calculated by counting the number of pixels above a certain threshold at the same *xy* position, across the layer of an image stack.

2. **Average thickness**: height of top biofilm pixel averaged for all pixels in acquisition area.

3. **Area coverage at each depth**: this is the area occupied by biomass at each optical section of the image stack. Pixels which contain biomass are those which are above the threshold value. It is computed by summing pixels above a certain threshold at each level as a percentage of the total pixels.

34

4. **Surface to volume ratio**: "The surface area to volume ratio calculation is performed by examining all voxels in the stack with biomass and by counting the surfaces that do not have a biomass-filled neighbour, do not face the substratum, or face a boundary of the confocal stack. All such surfaces are added up to give the total surface facing the void. The volume is derived from the *Biomass* function. The units are μm^2 for surface area and $\mu m^2/\mu m^3$ for surface/volume" (Heydorn *et al.*, 2016).

5. **Roughness co-efficient:** This is a dimensionless number that is indicative of the measure of the thickness variability across the entire image area. It is computed using thickness values according to the following equation

$$R_a^* = \frac{1}{N} \sum_{i=1}^{N} \frac{|L_{fi} - L_{fave}|}{L_{fave}} \tag{3.1}$$

Where L_i is the i'th individual thickness measurement, L_{fave} is the average thickness, and N is the number of the thickness measurements. Roughness co-efficient has been used as a measure of biofilm variability, with flat biofilms having a low roughness co-efficient.

Chapter 4

Results & Discussions

4.1 Biofilm Architecture

In describing the overall biofilm architecture, it is necessary to give and define a body of terms used to describe the biofilm structure that was observed. This body of terms is defined in Figure 4.1.1 in which a graphical summary of the biofilm architecture of the 6-day-old biofilms of *A. succinogenes* is given.

The structure of the 6- day-old biofilms of *A. succinogenes* was composed of cell microcolony pillars which varied considerably in thickness, area, and shape. Pillar diameter varied from 25 μm to 500 μm, as determined from quantitative analysis with COMSTAT, which was indicative of significant structural heterogeneity. Pillars rose all the way from the substratum surface, with a thickness range of 30– 300 μm, and consisted of a densely packed matrix of sessile cells. Furthermore, these pillars were characterised by having defined borders with an extensive network of channels separating them, as can be seen in Figure 4.1.2. This was characteristic of the heterogeneous mushroom-like model described in Section 2.3.

Figure 4.1.2 clearly depicts xy cross-sections of microcolony pillars surrounded by channels. The pillar area is growing with increasing height above the substratum

surface, corresponding to a decreasing width of the channels separating the pillars. This is characteristic of the mushroom-like pillar structure where a narrow stalk of biomass is attached to the substratum surface while a large microcolony of cells elevates into the bulk fluid.
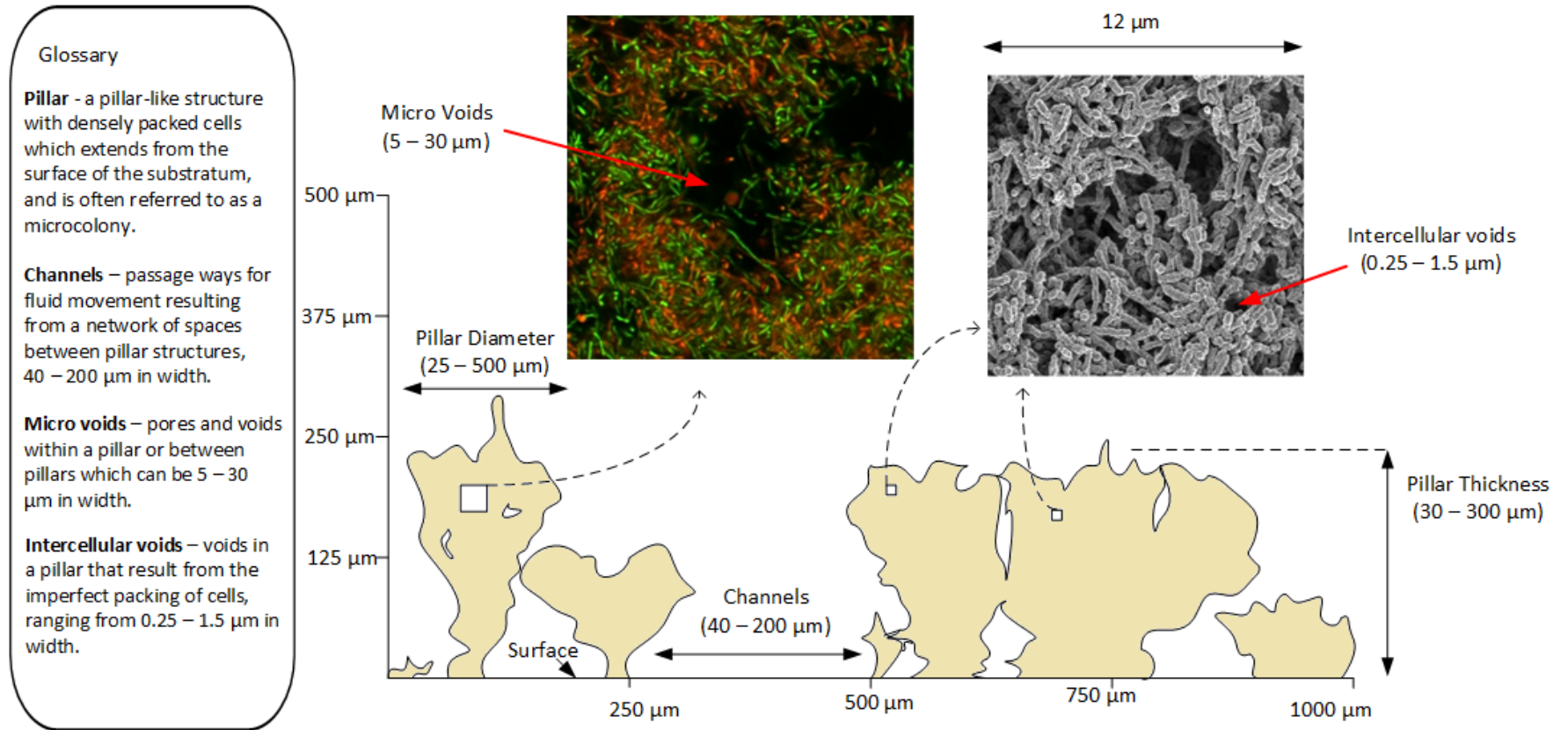
Figure 4.1.1: A generic graphical summary of the biofilm architecture observed along with a glossary defining the terminologies used.
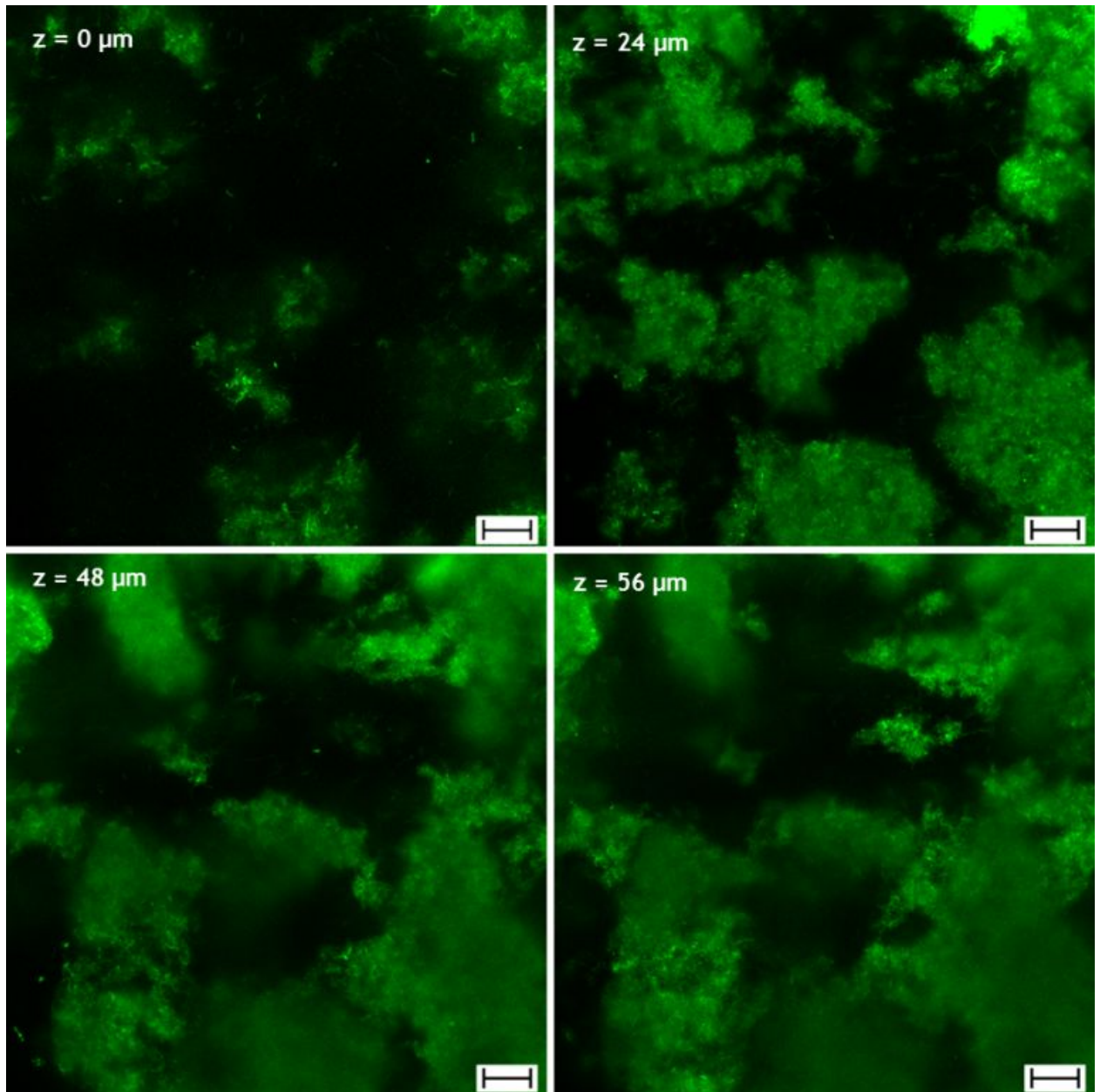
Figure 4.1.2: xy optical sections of a biofilm revealing cross sections of pillar structures. The pillar structures appear to be growing in diameter as they move away from the substratum surface at z = 0 µm. The scale bar denotes 20 µm .

39

Most of the pillars are separated by channels ranging from $40 - 200$ µm in width. However, some of the pillars coalesced, resulting in the formation of channels at deeper levels of the biofilm. This is evidenced in Figure 4.1.3 by the appearance of channels at the substratum surface ($z = 0$ µm) whereas they disappear at the top of the biofilm ($z = 28$ µm), indicating the presence of channels deeper into the biofilm and a coalescing of closely spaced pillars as the biofilm grows and matures. As such, both Figure 4.1.2 and Figure 4.1.3 show that the highest cross-sectional area of channels was deeper into the biofilm, indicating that biomass in the deeper layers is well supplied with growth media through these channels.
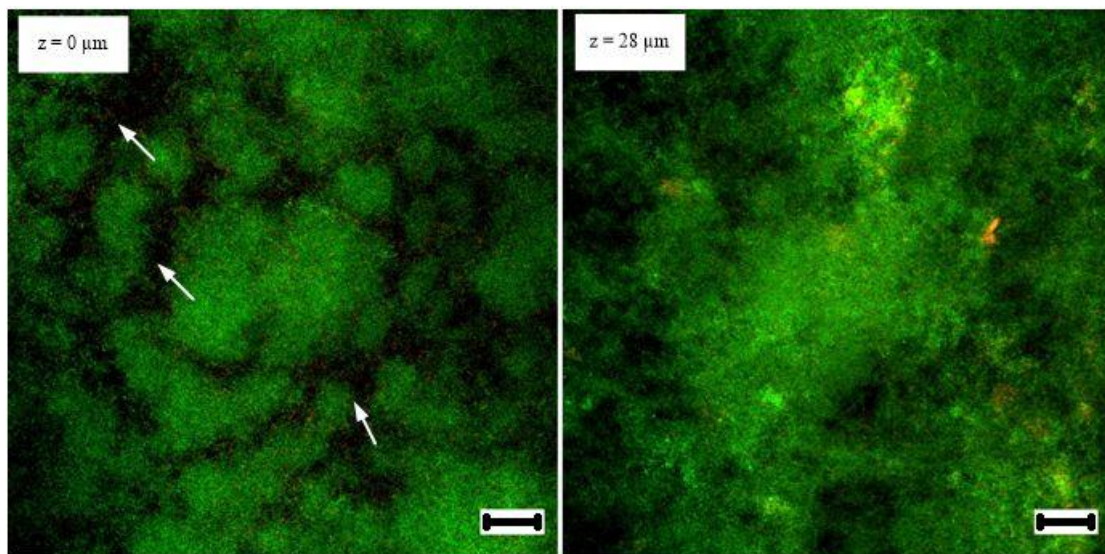
Figure 4.1.3: CSLM optical section images showing the appearance of channels at the substratum surface z = 0 µm, and their disappearance 28 µm above the surface of the substratum. Images were acquired as part of the 44 µm z stack at 4 µm depth increments. Scale bars indicate 50 µm

Figure 4.1.4 shows a 3D visualisation of the microcolony pillar structures as well as the top view of the 3D projection. The closely packed pillar structures can be seen with large elevated microcolonies towards the top of the biofilm. An xz sectional view of the mushroom-like pillar structures is also presented in Figure 4.1.5.
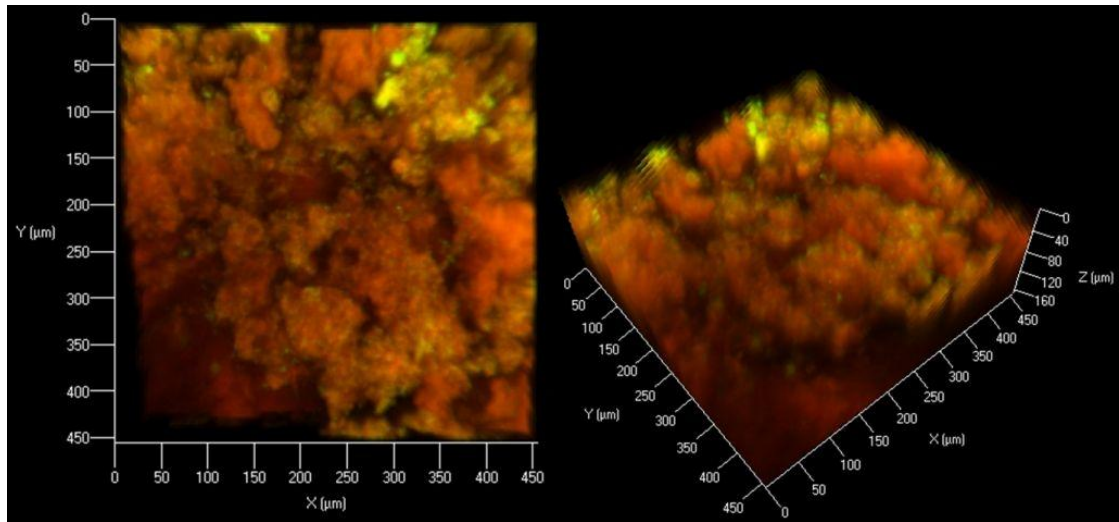
Figure 4.1.4: A top view and 3D visualisation of pillar structures in a biofilm. Images produced from reconstructions of optical scans acquired with CSLM.
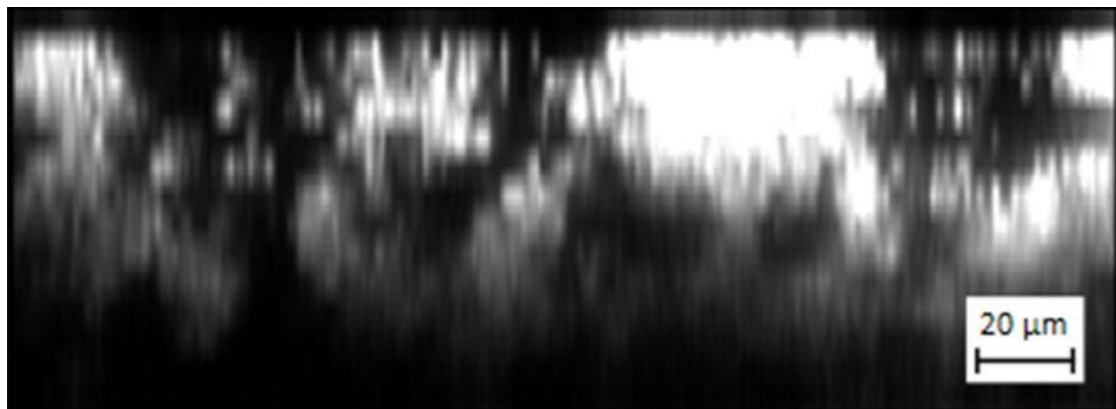
Figure 4.1.5: An xz sectional view of biofilm showing a cross-sectional view of the mushroom-like pillar structures. Image produced from orthographic views of a 3D stack acquired with CSLM.

41

A SEM topographical view of the biofilm pictured in Figure 4.1.6 also confirmed such a structure of closely spaced pillars with water channels separating them. SEM visualisation also revealed the presence of highly isolated pillars, with distances of approximately 200 μm and greater between them, as shown in Figure 4.1.6(A). However, this was rarely observed. A background single layer of cells, considerably lower in thickness than the pillars, covered the space between the highly isolated pillars. In areas where pillars were well separated, channels did not exist, only open spaces where the bulk fluid flowed freely.
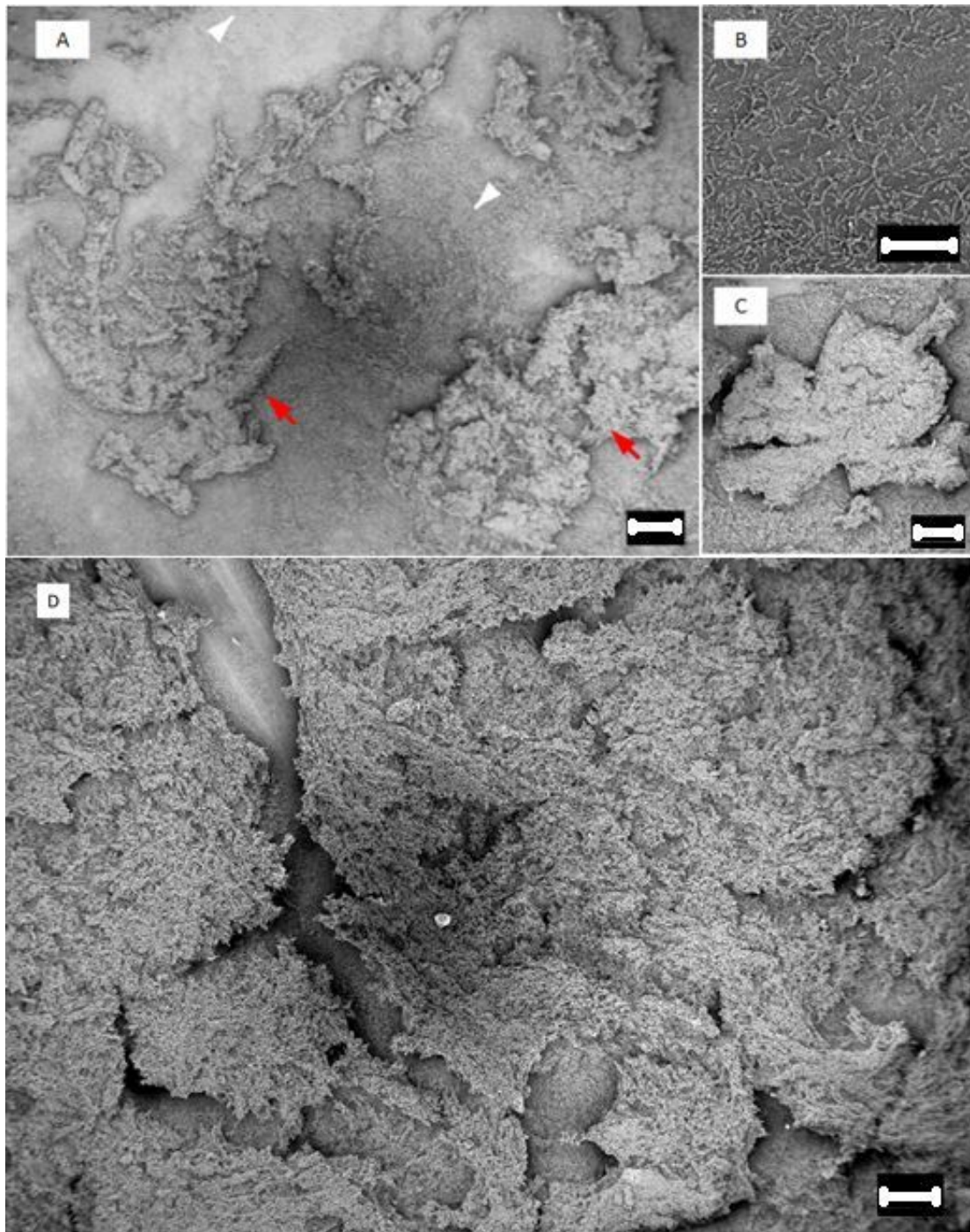
Figure 4.1.6: A SEM visualisation of an isolated pillar structure with a basal layer of cells (A), the white arrows are indicating a basal layer of cells. A close-up is shown in (B). The red arrows in (A) show the pillar structures, and the close-up is shown in (C). An example of closely spaced pillar structure separated by water channels is shown in (D). Scale bars in (A), (C) and (D) indicate 100 μm, whereas that in (B) indicates 10 μm.

43

Smaller channels could also be observed within pillars as seen in Figure 4.1.7, and were termed *micro voids*; they varied from 5 μm to 30 μm in width. While channels provide for nutrient flow around the pillars, micro voids provide for nutrient flow within the pillars, thereby reaching deeper sections within the pillars.
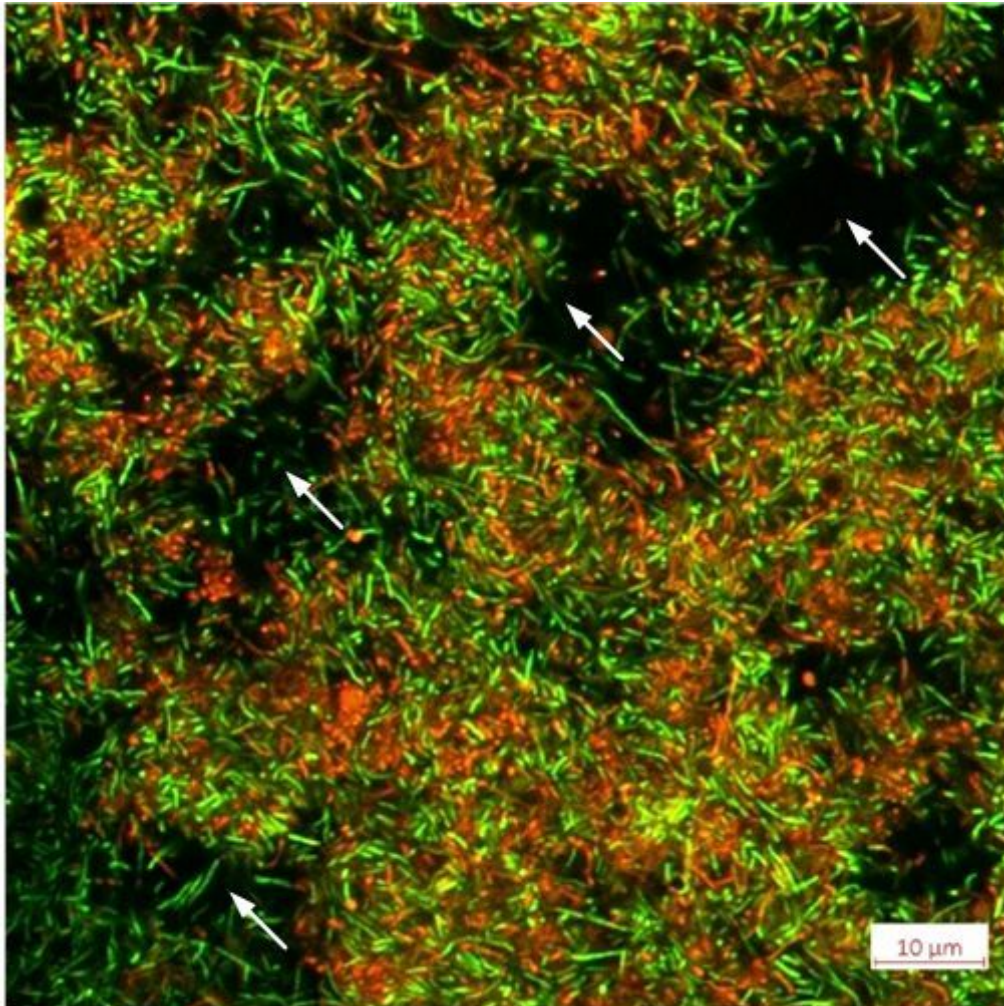
Figure 4.1.7: CSLM optical section image depicting the presence of micro voids within a pillar as indicated by the white arrows. Micro voids probably play a nutrient transport role to inner parts of the pillar.

Quantitative Analysis

Quantitative analysis of the biofilm structure was done with the COMSTAT image software. Several parameters can be calculated with COMSTAT, as explained in Section 3.6. Five CSLM image z-stacks, at a 100X magnification, were used for the quantitative analysis. This gave a total biofilm sampling area of 4.24×10^6 µm^2. A representative biofilm sampling area, as determined in Figure 3.6.1, is 2×10^6 µm^2. Thus, the analysis area is double the minimum representative biofilm sampling area. Automatic Otsu thresholding was selected, and a thousand connected biomass voxels were selected as a minimum colony size. Results are presented in Table 4.1.

Table 4.1: Summary of quantitative parameters

	Pillar Diameter (µm)	Roughness Coefficient	Average Thickness (µm)	Substratum Coverage(%)	Surface to Volume (µm^2/µm^3)
Mean	170±108[1]	0.54±0.21	92±35	33±13	0.25±0.07
Min	62	0.31	59	17	0.17
Max	470	0.91	200	49	0.38

[1] Standard deviation

Coverage at the substratum surface was consistently lower than 50% with an average of 33%, indicative of a tendency of the biofilm to aggregate and form microcolony pillars at the conditions investigated. The substratum coverage is similar to that determined in Figure 3.6.1. Approximation of the microcolony pillar cross-sectional area as circular gave a mean pillar diameter of 170 µm, although there was very large variation in pillar diameter ranging from 62 µm to 470 µm. On average five microcolonies were detected on substratum surface, at a 100x magnification. The microcolony pillars were thus mostly large in size, as was also observed in the SEM images. The mean average thickness of the five image stacks was 92

µm. However, the biofilm thickness varied from 30 to 300 µm. The low surface to volume ratios calculated with COMSTAT conform to the observed structure as it is expected that a biofilm structure composed of thick pillars with a large diameter will have low surface area to volume ratios.

Variation in biofilm thickness is best described by the surface roughness coefficient Ra^{*}, a parameter which is also mostly regarded as an indicator of biofilm structure heterogeneity (Murga, 1994). In their study of biofilm structures, Heydorn et al. (2016) observed that flat and fairly uniform structures of *Pseudomonas aeruginosa* were characterised by roughness values in the range of 0.15 – 0.35, as well as a 100% coverage of the substratum coverage. The same was observed by Murga (1994), with *P. aeruginosa* biofilms. However, a roughness coefficient range of 0.73 – 1.82 was observed for filamentous and elongated cell cluster biofilm structures of *Pseudomonas putida* biofilms (Heydorn *et al.*, 2000). In this way, a range of 0.31 – 0.91 in the surface roughness of *A. succinogenes* biofilms correctly reflects a structure characterised by closely spaced distribution of pillars separated by a network of water channels. This is because the range is in between the two extremes of a flat and uniform biofilm structure, and of a highly filamentous and elongated cell cluster biofilm structure.

Analysis for biofilm area coverage at each layer of the z stacks was also done, as shown in Figure 4.1.8. Although such an analysis is indicative of cellular density across the depth of biofilm, it can also reveal how the pillar structures grow.
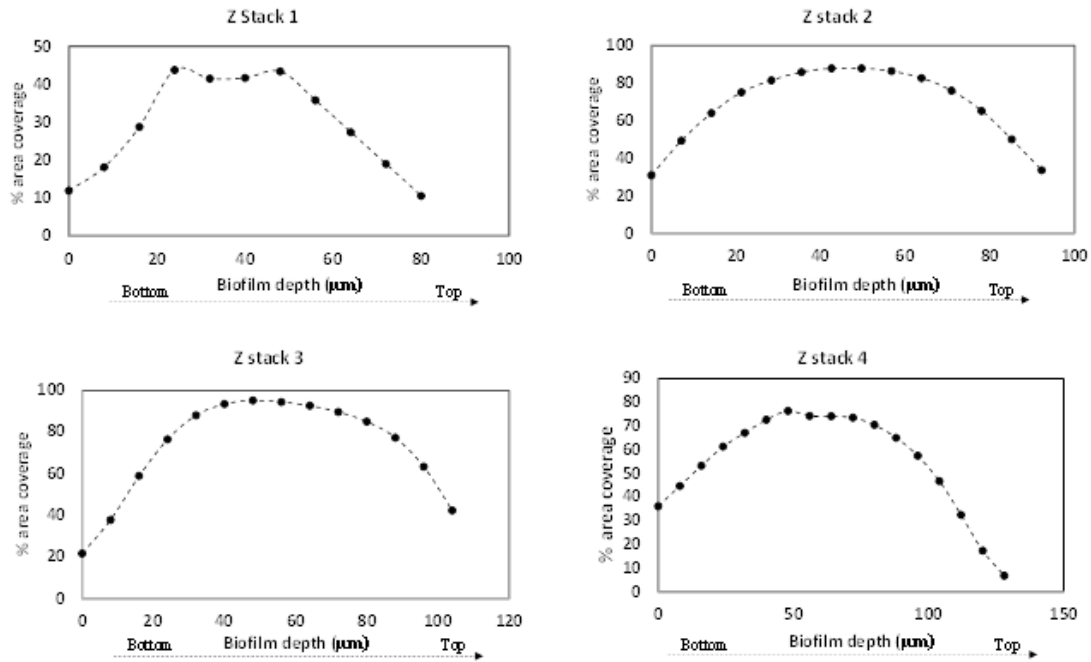
Figure 4.1.8:   Cross-sectional coverage of biofilm as function of biofilm depth. Observe the general trend of low coverage near the surface of the substratum and near the biofilm bulk liquid interface, whereas high coverage occurs approximately in the middle of the biofilm depth.

High cross sectional coverage of biofilm occurred in the middle part of the biofilm depth for each image stack. Low coverage was observed near the substratum surface and at the top of the biofilm surface. The rise in area coverage as the distance from the substratum coverage increases most probably represents a region where microcolony pillars are growing and expanding both sideways and upwards, thus occupying the space available to them. In this region, most of the pillars may coalesce to form pilars with an even larger diameter, and those that were further apart get closer together. This can also be witnessed in Figure 4.1.2 and Figure 4.1.3. The decrease in area coverage, resulting in low coverage at the top of the biofilm surface, can be attributed to the very large variation in the height of the microcolony pillars within a single stack. This variation in pillar thickness means that a smaller portion of the pillars are long, which results in lower coverage at the top part of the biofilm.

47

The results suggest that the widest channels are found in the deeper layers of the biofilm, due to the low biofilm area coverage found on these layers. Furthermore, the coverage curves suggest a pillar structure similar to the mushroom-like structures, of attached narrow stalks of biomass with a large microcolony of cells elevating into the bulk fluid, as discussed by Costerton (1995). It is expected that a biofilm structure made up of mushroom-like pillar structures will have lower area coverage near the surface of attachment, and that area coverage will increase with the height of the biofilm, as evidenced in Figure 4.1.8.

4.2 Cell Morphology

Light microscopic visualisation of suspended cells and detached pieces of biofilm in the reactor effluent showed that the cell morphology of planktonic and sessile cells is vastly different, as can be seen in Figure 4.2.1 . Planktonic cells were rod-shaped with a width range of $1 - 2$ µm and a length range of $4 - 5$ µm. On the other hand, sessile cells expressed an elongated rod morphology, and thus were much longer and thinner compared with planktonic cells, with lengths ranging from $5 - 100$ µm and a thickness range of $0.5 - 1$ µm. Using diameter and length dimensions of 2 x 5 µm and 1 x 100 µm for planktonic and sessile cells, respectively, meant that the surface area of one sessile cell was more than eight times higher than that of a planktonic cell, with double the surface to volume ratio. Visualisation with CSLM and SEM confirmed the sessile cell morphology of elongated rod-like shapes, as shown in Figure 4.2.2.
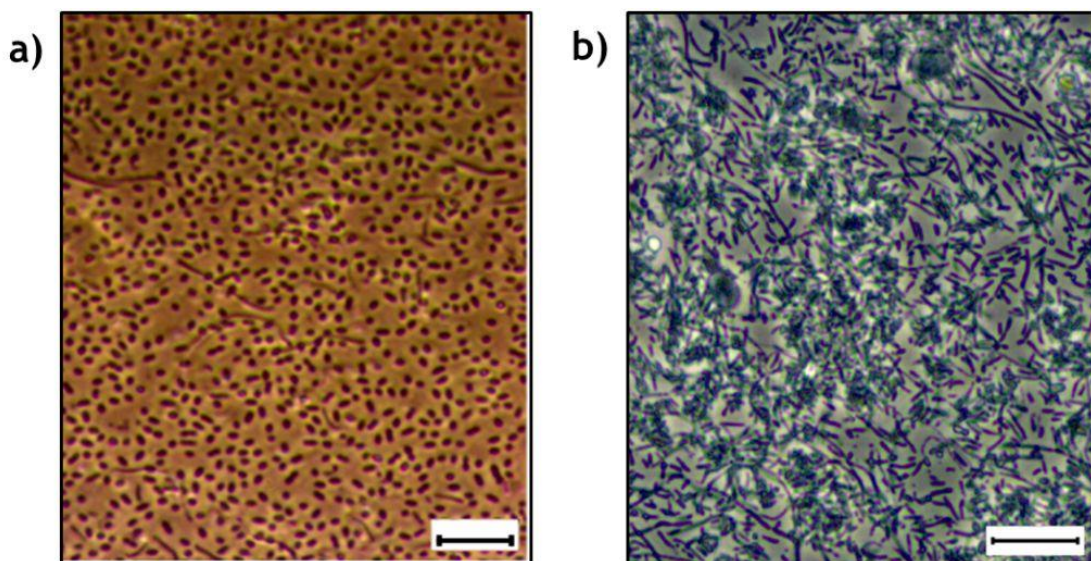

Figure 4.2.1: Light microscopy images showing distinct cell morphologies observed. Planktonic cells were rod-shaped as seen in (a). Sessile cells expressed an elongated rod morphology, and were thus much longer and thinner compared to planktonic cells, as seen in (b). Scale bars indicate 20 µm

The elongated rod morphology certainly gave sessile cells an advantage in terms

of nutrient uptake, due to the high surface to volume ratio. This adaptation was suitable for biofilm conditions, where mass transfer of nutrients and substrates like CO_2 is dominantly diffusion controlled, and thus large surface areas maximise nutrient uptake, especially for sessile cells located deep within a microcolony pillar. Moreover, the long cells in the biofilm result in considerable tangling within a micro-colony which adds to the structural stability of the pillar – an advantage that would be rather impossible to come by had the cells resembled a planktonic cell morphology. As such, *A. succinogenes* cells phenotypically expressed a morphology that most suited the conditions they found themselves in.
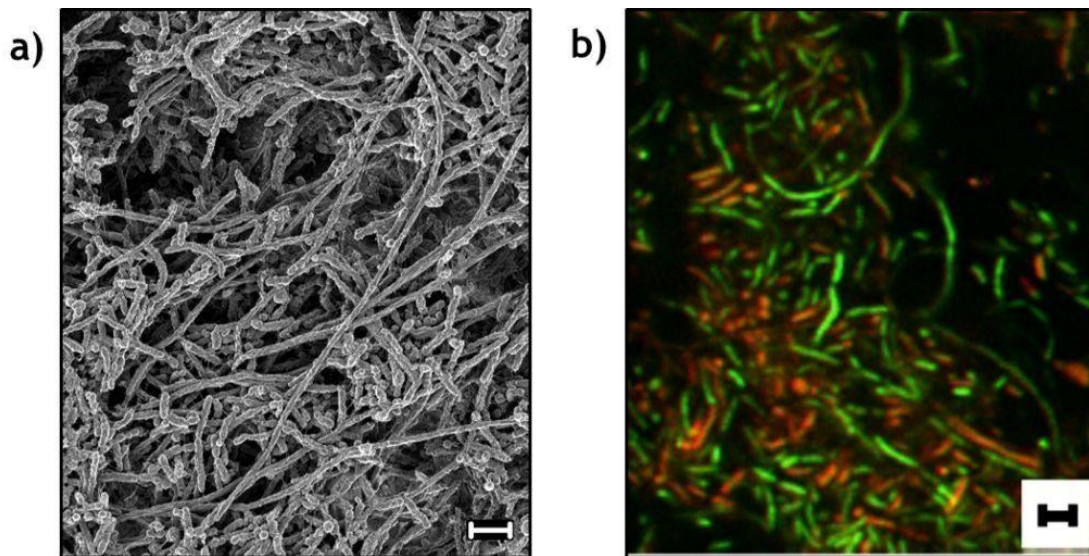
Figure 4.2.2: SEM micrograph showing the extended rod morphology of biofilm cells in (a), which were also observed with CSLM in (b). Scale bars indicate 2 μm

SEM visualisation at high magnification showed extensive cell-to-cell and cell-to-surface rod like connection wires, as shown in Figure 4.2.3. A closer inspection revealed that these connection wires extended from the cell surface, as indicated in Figure 4.2.3(b). Numerous wires extended from the surface of each sessile cell and connected either to other cell surfaces or to the substratum surface, depending on the location of the cell on the pillar. For sessile cells near the substratum surface, most connection wires contacted the substratum surface, as shown in Figure 4.2.3(a).

The presence of the fibre-like structures is characteristically noted in many biofilm investigations using traditional SEM sample preparation (Hunter & Beveridge, 2005; Dohnalkova *et al.*, 2010; Alhede *et al.*, 2012; Little *et al.*, 1991). Dohnalkova *et al.* (2010) speculated that these are collapsed EPS material, formed because of viscoelastic deformation of the EPS during the dehydration steps of traditional SEM sample preparation. However, it was also noted (as well as in this study) that fibre-like structures do not show any tapering at the points of connection, but appear as rod-like connections with a constant diameter (20 – 30 nm) across two connection points, an observation which is uncharacteristic of viscoelastic deformation. Nonetheless, Alhede *et al.* (2012), compared the two SEM techniques (cryo-SEM and traditional SEM), speculated that they could be either the condensed EPS material, or actual polymer substances found underneath the EPS matrix. This was mainly because when using cryo-SEM and ESEM, the hydrated EPS matrix is preserved, which prevents observation of internal EPS matrix components, and thus the absence or presence wire structures could not be confirmed.
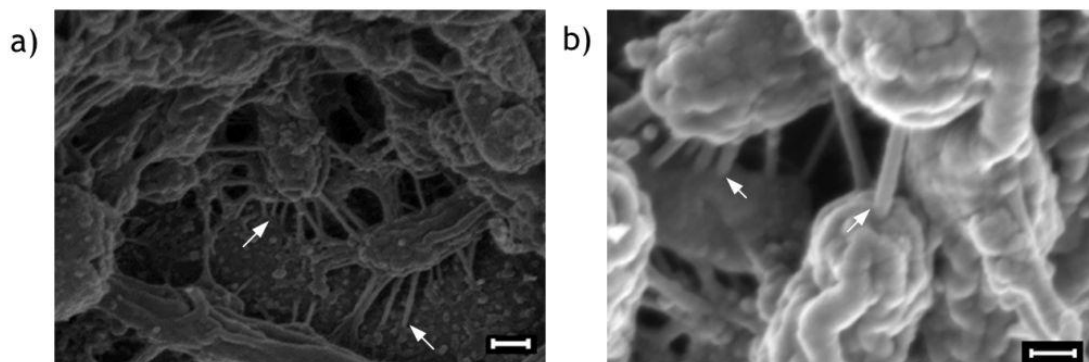
Figure 4.2.3: SEM visualisation revealed presence of thin constant diameter wire-like structures, approximately 20 – 30 nm in diameter, connecting cell surfaces to substratum surface (a), and to other cell surfaces (b). Significant mass deposits were also observed on the surface of biofilm cells. Scale bar in (a) indicates 100 nm and that in (b) indicates 200 nm.

Alternatively, these connection wires may be pili structures used in the conjugation process, a process reported to be much enhanced in biofilm bacterial life (Hausner & Wuertz, 1999). Interestingly, Ghigo (2001)demonstrated that the expression of conjugative pili in *E. coli* K12 accelerated both initial adhesion events and biofilm

development. It was further concluded that conjugate pilus act as an adhesion factor, allowing non-specific cell-to-surface or cell-to-cell contacts essential for microcolony development (Ghigo, 2001; Molin & Tolker-nielsen, 2003). It is therefore highly likely that these pili-like structures played the same role in the *A. succinogenes* biofilm, as evidenced by the pillar formations. Conjugative pili play a role in horizontal gene transfer by transferring plasmids to cells making contact with pili structures. If these fibre-like structures are indeed pili, then their role in the biofilm formation capacity of *A. succinogenes* should be investigated.

Molin & Tolker-Nielsen (2003) report that it is both EPS and conjugative pili which give the biofilm its structural stability under hydrodynamic conditions. SEM visualisation showed that there was material deposited on the cell surfaces as can be observed in Figure 4.2.3(b). We postulate that the deposited materials are exopolysaccharides which, before SEM preparation, probably occupied the space within intercellular voids–voids resulting from the imperfect packing of cells in microcolony pillars (see Figure 4.1.1). As the biofilm was dehydrated and dried during SEM sample preparation, the exopolysaccharides would have shrunk and deposited on the cell surface. Alternatively, it could be that the intercellular voids were filled with the bulk fluid and the EPS only covered the individual cell surfaces.

However, it can be argued that the pili connection structures would not have given the same structural stability to pillars had the cells resembled a planktonic cell morphology. The low surface area and length of planktonic cell morphology would not have permitted extensive pili connections. Therefore, it does seem that much exopolysaccharide production would have been required had the sessile cells maintained the planktonic cell morphology to enhance aggregation. Regions without wire connections between cells were also observed, as can be seen in Figure 4.2.4.
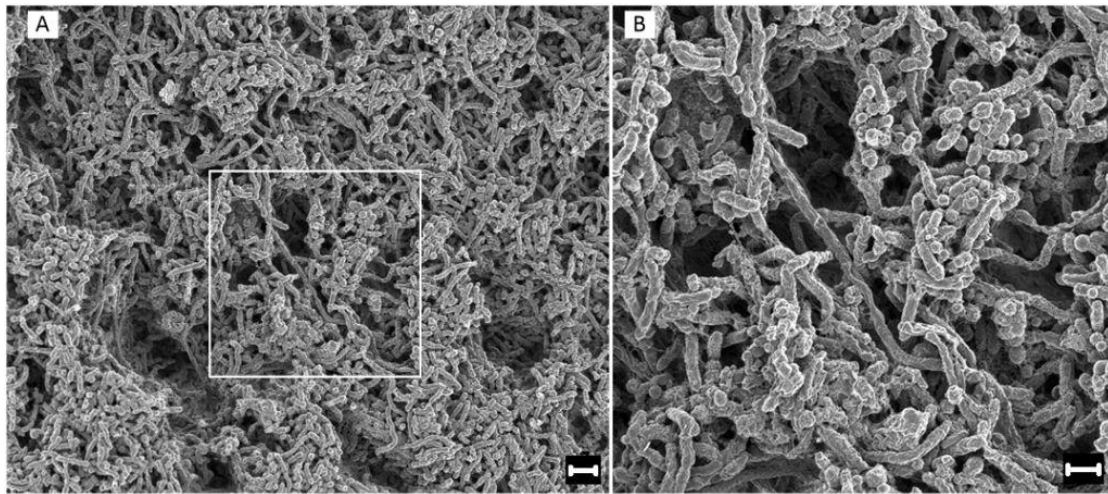
Figure 4.2.4: High cell density of pillars with no evident EPS (a), the white square is the enlarged micrograph on (b). Scale bar in (a) indicates 2 μm and that in (b) indicates 1 μm.

4.3 Cell Viability

In Figure 4.3.1, orthographic views of the biofilm at 100x magnification are presented. CSLM stack images were acquired at 100x magnification because of the relatively large acquisition area they offer, thus giving a more representative sample area in comparison to other magnifications. Dead portions of the biofilm are stained red, whereas living portions of the biofilm are stained green, as described in Section 3.6.There is a random scatter of living and dead portions of the biofilm across the xy plane. The same was observed with horizontal optical scans of other stack images taken at a 100x magnification. This is indicative of the various microenvironments, and hence the physiological states that exist in the biofilm, in both the vertical and horizontal planes.
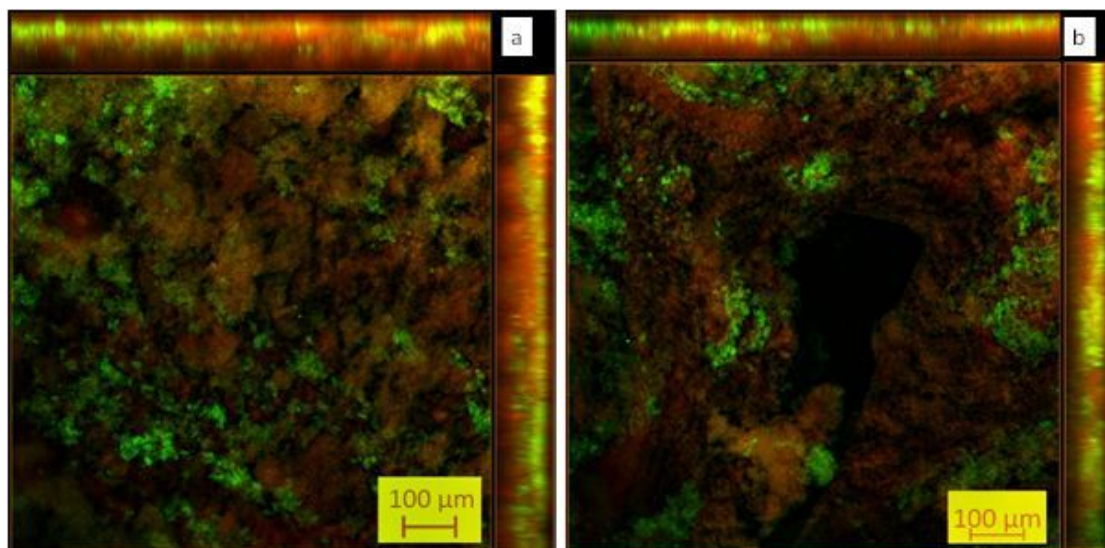

Figure 4.3.1: Variation of living and dead cells in the horizontal plane and the vertical plane. The images presented images are orthographic views of the xy, xz and yz planes. Observe the red (dead) layer of biofilm near the bottom of the yz and xz views of both (a) and (b), and in the top active layer.

54

A view of the vertical planes, xz and yz planes, presented in Figure 4.3.1, shows a dead layer of biofilm near the substratum surface and an active layer close to the top of the biofilm. A mean of the average percentage of dead cells count of each image stack revealed that 65% (with 2% standard deviation) of the entire biofilm was composed of dead cells. As is evident in Figure 4-13, most of the dead portion of the biofilm was in the bottom layers of the biofilm.

A closer inspection of the cells, at a 1000x magnification, in a microcolony pillar also revealed the same trend of increasing number of living cells towards the top part of the biofilm (see Figure 4.3.2). On average, in the bottom 20 μm layer of the biofilm, approximately 80% of the biofilm coverage is dead. However, the portion of covered area attributed to living cells began to increase past the middle of the biofilm towards the top part of the biofilm. A high percentage of living cells was thus found towards the top part of the biofilm. This can also be seen in Figure 4.3.3.
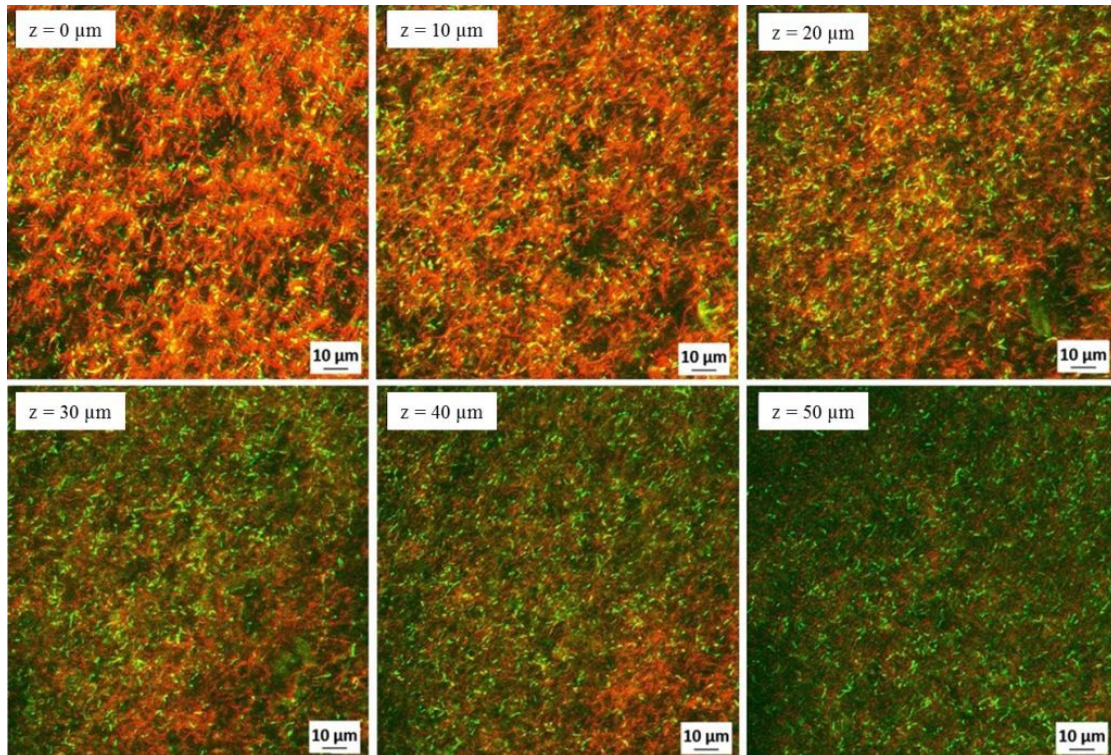
Figure 4.3.2: CSLM optical scans of the biofilm from the bottom of the substratum surface to the top part of the biofilm. Observe the increasing gradient of ling cells towards the top part of the biofilm.
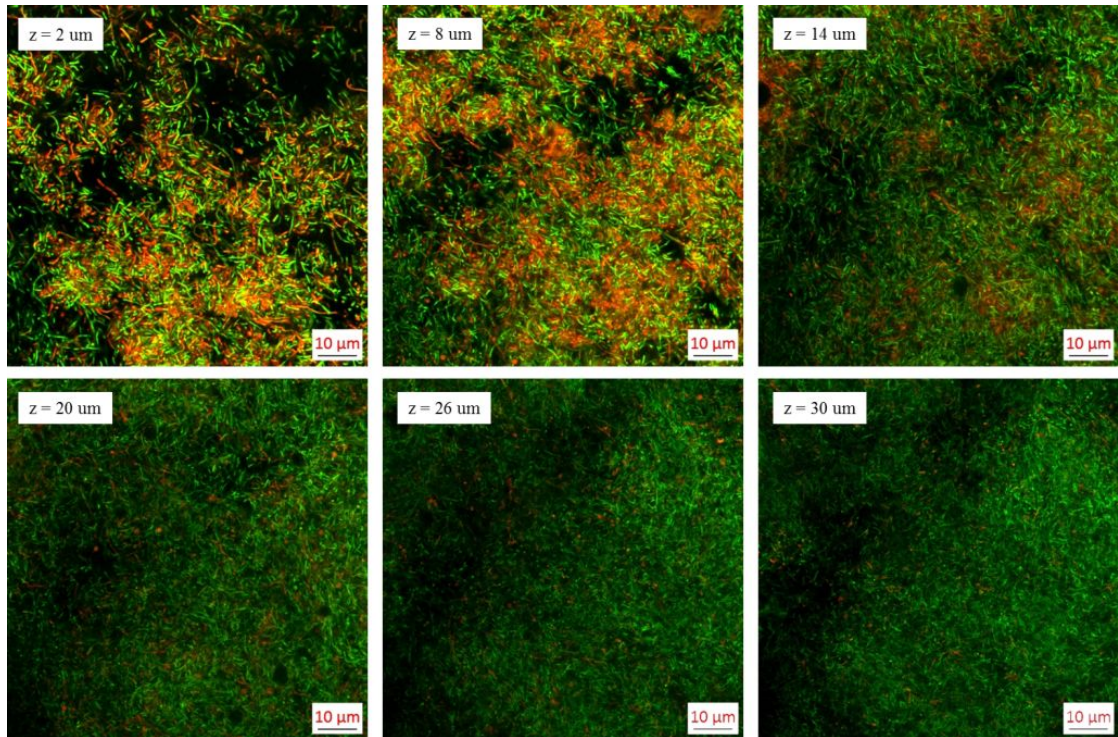
56

Figure 4.3.3: The increasing gradient of living cells with increase height above the substratum surface. Images were acquired with CSLM.

57

Although there is a random distribution of living and dead cells in the xy plane as seen in Figure 4.3.1, a clear trend could be observed in the vertical planes. The covered area is increasingly composed of more living cells moving away from the substratum surface. Since mass transfer in the biofilm is reported to be dominantly diffusion controlled (Loosdrecht et al., 2002), it can be expected that metabolite concentration will increase towards the bottom of the biofilm while the substrate concentration decreases. It can thus be assumed that the bottom layer of the biofilm is at high acid and low substrate conditions, whilst the top layer is at relatively low acid and high substrate conditions. Therefore, microenvironment conditions become increasingly favourable towards the top of the biofilm, hence the observed trend.

A close inspection of the xz and yz sections in Figure 4.3.1 shows a small layer of dead cells at the top part of the biofilm surface. The cause of this layer is unknown as it is expected that the tips of biomass at the top will be where most growth occurs, and thus should constitute more living cells. However, although care was taken to not let the biofilm dry during CSLM sample preparation, by covering the cover slips with a phosphate buffer solution after harvesting the samples from the reactor, it is possible that the topmost layers of the biofilm got dried. Nonetheless, it could also be that the top layer acts as a protective barrier for cells located in the middle part of the biofilm. Toxic substances in the medium would affect this layer first.

The biofilm was subjected to high acid conditions in the range of 15 – 21 g/L prior to sampling, and steady state was established at these conditions before sampling. Since it is known that at approximately 10 g/L SA concentration biofilm growth is inhibited, higher acid concentration could be the cause of such a high percentage of dead cells within the biofilm. It would be interesting to observe how this changes when steady state is established at lower acid conditions. However, the results show that operation at high acid conditions comes at a cost of low productivity due to decreased active biomass. In this way, a build-up of dead biofilm occurs in the reactor, occupying space without increasing productivity. This may also explain the occurrence of sudden biofilm detachment as the dead part of the biofilm may

easily become loose.

Appreciating that biofilm growth starts from the substratum surface and elevates into the bulk fluid, it can be assumed that most of the cells in the deeper layers of the biofilm are the oldest. It can further be said that these old cells have had prolonged exposure to acidic conditions in the fermenter. In this way, biofilm age most likely contributed to the cell viability state within the biofilms, as cell death was prominent at deeper layers of the biofilms.

Chapter 5

Conclusions & Recommendations

In this study, biofilms of *Actinobacillus succinogenes,* grown in a biofilm reactor system, were investigated through microscopic visualisation with CSLM and SEM. Biofilms were analysed when they were at pseudo steady state conditions in a productive mode. The objective was to visualise the structure formed by these biofilms as found in a bioreactor in high acid environment, and to analyse for the extent of cell death within these biofilms.

The structure of the 6-day-old biofilms of *A. succinogenes* was composed of cell micro-colony pillars which varied considerably in thickness, area, and shape. Pillars rose all the way from the substratum surface, and consisted of a densely packed matrix of sessile cells. These pillars were characterised by having defined borders with a network of channels, ranging from 40 µm to 200 µm in width, separating them. However, some of the pillars coalesced, resulting in the formation of channels at deeper levels of biofilm. Microcolony pillars were mostly large in size (average pillar diameter of 170 µm), and thicker with a mean thickness of 92 µm, although there was a large variability in biofilm thickness ranging from 30 µm to 300 µm. Moreover, low biofilm area coverage near the substratum surface suggested that widest water channels are found in the deeper layers of the biofilm.

Regarding cell morphology, very large differences were observed. Planktonic cells were rod-shaped whereas sessile cells expressed an elongated rod morphology, and thus were much longer and thinner compared with planktonic cells. The elongated rod morphology certainly gave sessile cells an advantage in terms of nutrient acquisition, due to the high surface to volume ratio, and the ability to tangle, thus reinforcing the pillar structures. Thin extensive rod-like connections were observed between cells, and between cell and surface. Different opinions are expressed in the literature regarding the identification of these connection structures. Dohnalkova *et al.* (2010) speculated that these are collapsed EPS material, formed because of viscoelastic deformation of the EPS during the dehydration steps of traditional SEM sample preparation. On the other hand, Alhede *et al.* (2012) suggested that they could be either the condensed EPS material, or actual polymer substances found underneath the EPS matrix, since modern techniques such as cryo-SEM and ESEM preserve the hydrated EPS matrix thus preventing observation of internal EPS matrix components.

Viability stains showed that, on average, in the bottom 20 μm layer of the biofilm, 80% of the biofilm coverage is dead. However, the portion of covered area attributed to living cells began to increase past the middle of the biofilm towards the top part of the biofilm. A high percentage of living cells was thus found towards the top part of the biofilm. Overall, 65% (with 2% standard deviation) of the entire biofilm was composed of dead cells. In this way, the results show that operation at high acid conditions comes at a cost of low productivity due to decreased active biomass. Therefore, a build-up of dead biofilm occurs in the reactor, occupying space without increasing productivity.

This research revealed the structure of biofilms formed by *A. succinogenes* in high acid concentration environments of a bioreactor, and the bacterial viability within these biofilms. It is recommended that the *A. succinogenes* biofilm development process be studied so that changes occurring to the structure as acid conditions build up in the reactor are tracked. The influence of reactor conditions, such as shear rates, and acid conditions on this structure will also give valuable insight into the overall bio-succinic process. More importantly, the use of artefacts-free

techniques such as cryo-SEM and ESEM should be employed as this will aid in drawing accurate conclusions.

Chapter 6

References

Alhede, M., Qvortrup, K., Liebrechts, R., Hoiby, N., Givskov, M. & Bjarnsholt, T. 2012. Combination of microscopic techniques reveals a comprehensive visual impression of biofilm structure and composition. *Immunol Med Microbiol*, 65 (2) pp. 335–342

Beauprez, J.J., De Mey, M. & Soetaert, W.K. 2010. Microbial succinic acid production: Natural versus metabolic engineered producers. *Process Biochem*, 45(7), pp. 1103–1114.

Bradfield, M.F.A & Nicol, W. 2014. Continuous succinic acid production by *Actinobacillus succinogenes* in a biofilm reactor: Steady-state metabolic flux variation. *Biochem Eng Journal*, 85: pp. 1–7.

Bradfield M.F.A, Mohagheghi, A., Salvachúa, D., Smith, H., Black, B.A., Dowe, N., Beckham, G.T.& Nicol, W. 2015. Continuous succinic acid production by *Actinobacillus succinogenes* on xylose-enriched hydrolysate. *Biotechnol Biofuels*, 8(1), pp. 181. doi:10.1186/s13068-015-0363-3

Bradfield, M.F.A, & Nicol, W. 2016. Continuous succinic acid production from xylose by *Actinobacillus succinogenes*. *Bioprocess Biosyst Eng*, 39, pp. 233–244. doi:10.1007/s00449-015-1507-3

Bradfield, M.F.A. & Nicol, W. 2016. The pentose phosphate pathway leads to enhanced succinic acid flux in biofilms of wild-type *Actinobacillus succinogenes*. *Appl Microbiol Biotechnol*, 100, pp. 9641–9652. doi:10.1007/s00253-016-7763-6

Brink, H.G. & Nicol, W. 2014. Succinic acid production with *Actinobacillus succinogenes*?: Rate and yield analysis of chemostat and biofilm cultures. *Microb Cell Fact*, 13, pp. 111–123.

Cerca, N., Gomes, F., Pareira, S., Teixeira, P. & Oliveira, R. 2012. Confocal laser scanning microscopy analysis of *S. epidermidis* biofilms exposed to farnesol, vancomycin and rifampicin. *BMC Res Notes*, 16(5), pp. 244. doi:10.1186/1756-0500-5-244.

Cheng, K., Demirci, A. & Catchmark, J.M. 2010. Advances in biofilm reactors for production of value-added products. *Appl Microbiol Biotechnol*, 87(2), pp. 445–456.

Cherubini, F. 2010. The biorefinery concept: Using biomass instead of oil for producing energy and chemicals. *Energy Convers Manage*, 51(7), pp. 1412–1421.

Cok, B., Tsiropoulos, I., Roes, A.L. & Patel, M.K. 2014. Succinic acid production derived from carbohydrates?: An energy of a platform chemical toward a bio-based economy. *Biofuels, Bioprod Biorefin*, 8(1), pp. 16–29.

Conchello, J.-A. & Lichtman, J.W. 2005. Optical sectioning microscopy. *Nature Methods*, 2(12), pp. 920–931.

Costerton, J.W., Lewandowski, Z., Caldwell, D.E., Korber, D.R. & Lappin-Scott, H.M. 1995. Microbial biofilms. *Ann Rev Microbiol*, 47, pp. 711–745.

Costerton, J.W. 1999. Introduction to biofilm. *Int J Antimicrob Ag*, 11(3?4), pp. 217–221.

Davey, M.E. & O?Toole, G.A. 2000. Microbial biofilms: From ecology to molecular genetics. *Microbiol Mol Biol Rev*, 64(4), pp. 847–67.

Demirbas, M.F. 2009. Biorefineries for biofuel upgrading: A critical review. Appl Energy, 86, pp. 151–161. Available at: http://dx.doi.org/10.1016/j.apenergy.2009.04.043.

Dohnalkova, A.C., Marshall, M.J., Arey, B.W., Williams, K.H., Buck, E.C. & Fredrickson, J.K. 2011. Imaging hydrated microbial extracellular polymers: comparative analysis by electron microscopy. *Appl Environ Microbiol*, 77(4), pp. 1254–1262.

Donlan, R.M. 2009. Preventing biofilms of clinically relevant organisms using bacteriophage. *Curr Trends Microbiol*, 17(2), pp. 66–72.

Fitzpatrick, M., Champagne, P., Cunningham, M.F. & Whitney, R.A. 2010. Bioresource technology ? A biorefinery processing perspective: Treatment of lignocellulosic materials for the production of value-added products. *Bioresour Technol*, 101(23), pp. 8915–8922.

Flemming, H., Wingender, J., Szewzyk, U., Steinberg, P., Rice, S.A. & Kjelleberg, S. 2016. Biofilms: an emergent form of bacterial life. *Nature Publishing Group*, 14(9), pp. 563–575.

Flemming, H. & Wingender, J. 2010. The biofilm matrix. *Nat Revs Microbiol*, 8(9), pp. 623–633.

Fletcher, M. 1986. Measurement of glucose utilization by *Pseudomollas fluorescells* that are free-living and that are attached to surfaces. *Appl Environ Microbiol*, 52, pp. 672–676.

Ghatak, H.R. 2011. Biorefineries from the perspective of sustainability: Feedstocks, products, and processes. *Renew Sustainable Energy Rev*, 15(8), pp. 4042–4052.

Ghigo, J. 2001. Natural conjugative plasmids induce bacterial biofilm development. *Nature*, 412, pp. 442–445.

Gross, R., Hauer, B., Otto, K. & Schmid, A. 2007. Microbial biofilms: New catalysts for maximizing productivity of long-term biotransformations. *Biotechnol*

Bioeng, 98(6), pp. 1123–1134.

Guettler, M., Rumler, D. & Jain, M. 1999. *Actinobacillus succinogenes* sp. nov., a novel succinic-acid-producing strain from the bovine rumen. *Int J System Bacteriol*, 49, pp. 207–216.

Hausner, M. & Wuertz, S. 1999. High rates of conjugation in bacterial biofilm development. *Appl Environ Microbiol*, 65(8), pp. 3710–3713.

Herselman, J., Bradfield, M.F.A, Vijayan, U.R.P. & Nicol, W. 2017. The effect of carbon dioxide availability on succinic acid production with biofilms of *Actinobacillus succinogenes*. *Biocheml Eng*, 117, pp. 218–225.

Heydorn, A., Nielsen, A.T., Hentzer, M., Sternberg, C., Givskov, M., Ersboll, B.J. & Molin, S. 2000. Quantification of biofilm structures by the novel computer program COMSTAT. *Microbiol UK*, 146, pp. 2395–2407.

Hunter, R.C. & Beveridge, T.J. 2005. High-resolution visualization of Pseudomonas aeruginosa PAO1 biofilms by freeze-substitution transmission electron microscopy. *J Bacteriol*, 187(22), pp. 7619–7630.

Korber, D.R., Lawrence, J.R., Hendry, M. J. & Caldwell, D.E. 1992. Programs for determining statistically representative areas of microbial biofilms. *Binary*, 4, pp. 204–210.

Lee, P.C., Lee, S.Y, Hong, S.H. & Chang, H.N. 2002. Isolation and characterization of a new succinic acid-producing bacterium, *Mannheimia succiniciproducens* MBEL55E, from bovine rumen. *Appl Microbiol Biotechnol*, 58(5), pp. 663–668.

Little, B., Wagner, Ray, R & Pope, R. 1991. Biofilms?: An ESEM evaluation of artifacts introduced during SEM preparation. *J Ind Microbiol*, 8(4), pp. 213–221.

Loosdrecht, M.C.M., Heijnen, J.J., Eberl, H., Kreft, J. & Picioreanu, C. 2002. Mathematical modelling of biofilm structures. *Antonie Van Leeuwenhoek*, 81(245), pp. 245–256.

McKinlay, J.B., Zeikus, J.G. & Vieille, C. 2005. Insights into *Actinobacillus suc-cinogenes* fermentative metabolism in a chemically defined growth medium. *Appl Environ Microbiol*, 71(11), pp. 6651–6656.

Molin, S.M. & Tolker-Nielsen, T. 2003. Gene transfer occurs with enhanced effi-ciency in biofilms and induces enhanced stabilisation of the biofilm structure. *Curr Opin Biotechnol*, 14, pp. 255–261.

Neu, T.R. & Lawrence, J.R. 2015. Innovative techniques, sensors, and approaches for imaging biofilms at different scales. *Curr Trends Microbiol*, 23(4), pp. 233–242.

Parsek, M.R. & Tolker-Nielsen, T. 2008. Pattern formation in *Pseudomonas au-reginosa* biofilms. *Curr Opin Microbiol*, 11(6), pp. 560–566.

Pateraki, C., Patsalou, M., Vlysidis, A., Kopsahelis N., Webb, C., Koutinas, A.A. & Loutinas, M. 2016. *Actinobacillus succinogenes*: Advances on succinic acid production and prospects for development of integrated biorefineries. *Biochem Eng*, 112, pp. 285–303.

Qureshi, N., Annous, B.A., Ezeji, T.C., Karcher, P. & Maddox, I.S. 2005. Biofilm reactors for industrial bioconversion processes: Employing potential of enhanced reaction rates. *Microb Cell Fact*, 4, p. 24.

Samuelov, N., Datta, R., Jain, M.K. & Zeikus, J.G. 1999. Whey fermentation by *Anaerobiospirillum succiniciproducens* for production of a succinate-based animal feed additive. *Appl Environ Microb*, 65(5), pp. 2260–2263.

Scholten, E., Renz, T. & Thomas, J. 2009. Continuous cultivation approach for fermentative succinic acid production from crude glycerol by *Basfia succinicipro-ducens* DD1. *Biotechnol Lett*, 31(12), pp. 1947–1951.

Shotton, D.M. 1989. Confocal scanning optical microscopy and its applications for biological specimens. *J Cell Sci*, 94, pp. 175–206.

Stewart, P.S., Peyton, B.M. & Drury, W.J. 1993. Quantitative observations of heterogeneities in *Pseudomonas aeruginosa* biofilms. *Appl Environ Microbiol* 59,

pp. 327–329.

Thomas, D. 2009. Biorefinery: Toward an industrial metabolism. *Biochimie*, 91(6), pp. 659–664.

Urbance, S.E., Pometto, A.L., DiSpirito, A.A. & Dermici, A. 2003. Medium evaluation and plastic composite support ingredient selection for biofilm formation and succinic acid production by *Actinobacillus succinogenes*. *Food Biotechnol*, 17(1), pp. 53–65.

Venugopalan, V.P., Kuen, M., Hausner, M., Spring, D., Wilderer, P.A. & Wuertz, S. 2005. Architecture of a nascent *Sphingomonas* sp. biofilm under varied hydrodynamic conditions. *Appl Environ Biotechnol*, 71(5), pp. 2677–2686.

Vu, B., Chem, M., Crawford, R.J. & Ivanova, E.P. 2009. Bacterial extracellular polysaccharides involved in biofilm formation. *Molecules*, 14(7), pp. 2535–2554.

Walker, J.T., Mackerness, C.W., Rogers, J. & Keevil, C.W. 1995. Heterogeneous mosaic biofilm: A haven for waterborne pathogens. In: Lappin-Scott, H.M. & Costeron, J.W. (Eds.), *Microbial Biofilms*. Cambridge: Cambridge University Press, pp. 196–204.

Wimpenny, J.W.T. & Colasanti, R. 2006. A unifying hypothesis for the structure of microbial biofilms based on cellular automaton models. *FEMS Microbiol Ecol*, 22(1), pp. 1–16.

Wolfaardt, G.M., Lawrence, J.R., Robarts, R.D., Caldwell, S.J. & Caldwell, D.E. 1994. Multicellular organization in a degradative biofilm community. *Appl Environ Microbiol*, 60(2), pp. 434–446.

Wu, Y., Liang, J., Rensing, K., Chou, T. & Libera, M. 2014. Extracellular matrix reorganization during cryo preparation for scanning electron microscope imaging of *Staphylococcus aureus* biofilms. *Microsc Microanal*, 20(5), pp. 1348–1355.

Yang, X., Beyenal, H., Harkin, G. & Lewandowski, Z. 2000. Quantifying biofilm structure using image analysis. *Microbiol Meth*, 39, pp. 109–119.